

Plasma actuators for aeronautics applications - State of art review-

G. Touchard

Laboratoire d'Etudes Aérodynamiques, Boulevard Marie et Pierre Curie, BP 30179,
86962 Futuroscope Cedex, France

Abstract - The goal of this paper is to make a detailed review of the designs and associated setups of the different aerodynamic plasma actuators developed these last twenty years. First, some basic aspects of aerodynamic and their consequences in aeronautics are exposed. Then, the different aerodynamic conventional and plasma actuators are presented. Finally, the limits and the prospects of plasma actuators considered for airflow control are discussed.

Keywords - Air flow control, plasma actuators.

I. INTRODUCTION

It is now well known and many papers have already been published in the "International Journal of Plasma Environmental Science & Technology" (IJPEST), that non thermal plasma can be used for environmental applications; even some joint research between our laboratory and the "Department of Ecological Engineering" of Toyohashi University of Technology, Japan, has already been made concerning surface barrier discharge and specially sliding discharge [1]. This paper concerns another environmental purpose using plasma applications: the fuel consumption reduction or air planes enhancing the aerodynamic flow control with plasma actuators. Recent researches and developments on aerodynamic plasma actuators is due to the conjunction of a technological need in aerodynamic control to be used in aeronautic industry and new investigations on aerodynamic properties of plasma actuators. In order to understand the reasons of the recent important development of researches on plasma actuators it is first important to know the technological need in air flow control for aeronautic applications.

II. TECHNOLOGICAL NEED IN AIRFLOW CONTROL FOR AERONAUTIC APPLICATIONS

This paragraph deals with the basic knowledge which is needed to understand the aerodynamic phenomena that has to face aeronautic industry. Most of the results presented here are well developed in two reference books written by Schlichting [2], and Comolet [3].

A. Aerodynamic forces

A plate placed perpendicular to an air flow is submitted to a force which push the plate in the same direction that the flow (figure 1). It is due to the difference between the total pressures on the two sides of the plate. Indeed, behind the plate the pressure is lower due to the detachment of the flow. In aeronautics this force is generally called the drag.

If the plate is inclined (figure 2) the force has a

vertical component. In aeronautics this component is called the lift. Finally an airfoil, which can correspond for instance to the wings of an airplane, moving from right to left is generally submitted to two different forces: one from left to right (so in the opposite direction of the motion) called the drag and one from bottom to top called the lift (figure 3).

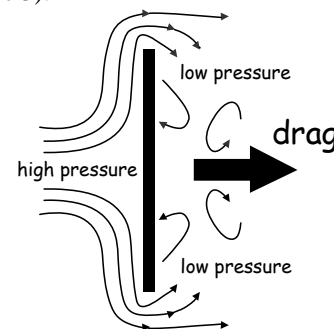


Fig. 1. Force on a vertical plate submitted to a flow.

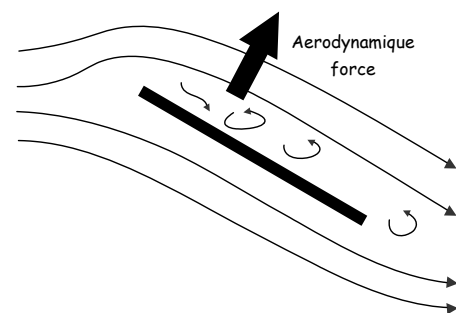


Fig. 2. Force on an inclined plate submitted to a flow.

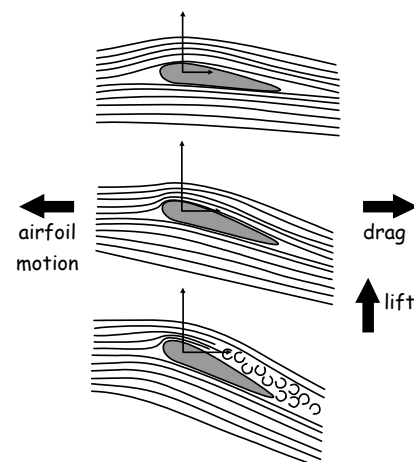


Fig. 3. Drag and lift on an airfoil submitted to a flow.

Corresponding author: G. Touchard
e-mail address: Gerard.Touchard@lea.univ-poitiers.fr

Received; January 16, 2008, Accepted; March 18, 2008

Thus, if we consider an airplane in motion at a constant velocity and altitude (figure 4), the drag is equal and opposite to the traction due to the propeller moved by the engine and the lift is equal and opposite to the weight due to the gravity. The drag is due to the friction of the air on the airplane body, the wings and the tail. The lift is essentially due to the friction on the wings. Then, it is important to try to reduce the drag during takeoff and cruise but not for landing and to control the lift, as a higher lift is needed during takeoff than for cruise or landing. Anyway, the shape of the different part of a plane are designed in order to have an aerodynamic profile, which means a drag as small as possible and the appropriate lift for takeoff, cruise and landing. An airplane is made of different parts submitted to air flows. Each of them constitutes an airfoil.

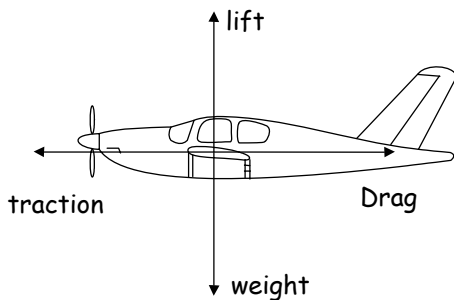


Fig. 4. Aerodynamic forces on an airplane in motion.

B. Airfoil example: the wings of an airplane

As the wings are mandatory parts of an airplane, it is important to examine the profile of these airfoils. The wings of an airplane are airfoils which must generate a drag as small as possible and a lift equal to the weight of the plane for a given inclination and velocity. After a lot of studies (Betz [4], Jones [5]), some profiles of airfoils have been designed to fulfill this purpose. The most known are those proposed by the National Advisory Committee for Aeronautics (NACA). Furthermore, this committee gave a classification of airfoils profiles. One of the most used to design wings is the NACA four-digit series [6]. As an example the profile NACA00xx is related to a profile without camber and xx indicates the value of the maximum thickness in percentage of the width of the wing called usually the chord. We see in figure 5 the profile of a NACA0015 airfoil (the maximum thickness is 15% of the chord).

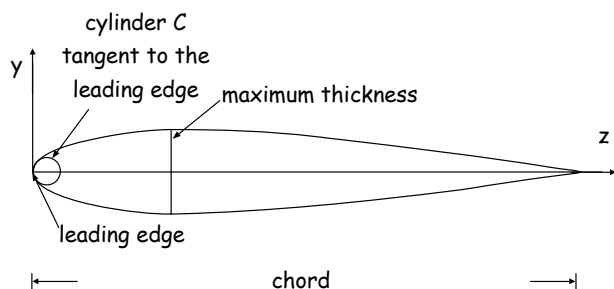


Fig. 5. NACA 00xx profile.

The profile of the NACA 00xx is symmetrical regarding the z axis, and the value of y may be computed

with the following formula:

$$y = \left(\frac{xx}{0.2} \right) \left(0.2969 \sqrt{z} - 0.126 z - 0.3516 z^2 \right) + 0.2843 z^3 - 0.1015 z^4 \tag{1}$$

z is the position along the chord and vary from 0 to 1, y is the half thickness at a given value of z (median line to surface) and xx is the maximum thickness in percentage of the chord. The leading edge is tangent to a cylinder the radius of which r is given by:

$$r = 1.1019 xx^2 \tag{2}$$

Such symmetrical airfoil presents no lift when its median line is parallel to the flow, this is the reason why other airfoils have been performed with a camber of the median line. The simplest asymmetric airfoils are the NACA four digits series, which used the same formula as that used to generate the 00xx symmetric foils, but with the line of mean camber bent. Thus a NACA mpxx has a profile similar to the NACA 00xx but where m is the maximum camber in percentage of the chord and p is the distance from the leading edge of this maximum in tenths of the chord

The formula used to compute the mean camber line is given by:

$$\text{from } x = 0 \text{ to } x = p: \quad y = \frac{m}{p^2} (2 p x - x^2) \tag{3}$$

$$\text{from } x = p \text{ to } x = 1: \quad y = \frac{m}{(1-p)^2} (1 - 2 p + 2 p x - x^2) \tag{4}$$

As an example we can see in figure 6 a NACA 2312 profile



Fig. 6. NACA 2312 profile.

Such profile presents a lift even if the z axis is parallel to the air flow (zero angle of attack). Nevertheless, a symmetric airfoil NACA00xx generates a lift for a non null angle of attack (figure 7). Very often experiments are made with a symmetric profile and specially a NACA 0015 (often called just NACA15).

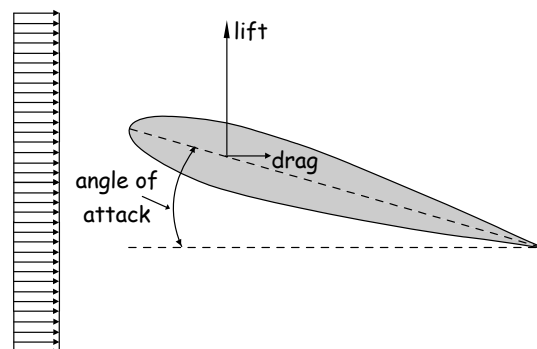


Fig. 7. Lift and drag on a NACA 0015 profile with attack angle.

C. Boundary layer

We are now going to examine the effect of the airflow around a body to understand better the need of aerodynamic actuators.

A vehicle in motion is submitted to the friction of the air around its body. This is due to the attachment of the air molecules at the interface air/body which induces a null relative velocity of the air at this interface, then, the viscosity of the air produces the so called "boundary layer" all around the body in motion. In this layer the relative velocity of air around the body evolves from zero at the body wall, to a constant velocity far from the body. This relative external velocity is equal and opposite from the body velocity. We first are going to examine the boundary layer development on a flat plate.

D. Boundary layer on a flat plate

We consider a flat plate and a uniform flow velocity U_∞ before the plate (figure 8). Then from the beginning of the plate (generally called the leading edge) a laminar boundary layer develops. The width of this layer is increasing with the distance to the leading edge. At the limit of the boundary layer the velocity is U_∞ . (in practice, the limit is defined when the velocity is $0.99 U_\infty$). The pressure is more important upstream that downstream, we say that the pressure gradient is negative. The velocity profile depends on the flow regime. Indeed two flow regimes exist: the laminar flow and the turbulent flow with a transition between laminar to turbulent. The profile given in figure 8 corresponds to a laminar flow.

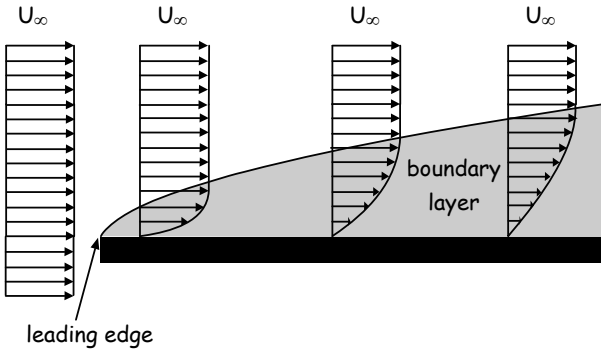


Fig. 8. Laminar boundary layer development on a flat plate.

At a given distance from the leading edge the transition from laminar to turbulent appears. This transition to turbulence is clearly discernible by a sudden and large increase of the boundary layer thickness (figure 9). Considering the Reynolds number $R = \frac{U_\infty x}{\nu}$, (where U_∞ is the external velocity, x the distance from the leading edge and ν the air kinematic viscosity), then the transition on a flat plate appears for the so called critical value of the Reynolds number $R_c \approx 3.2 \cdot 10^5$. In the case of an airfoil the same phenomenon occurs with roughly the same characteristics.

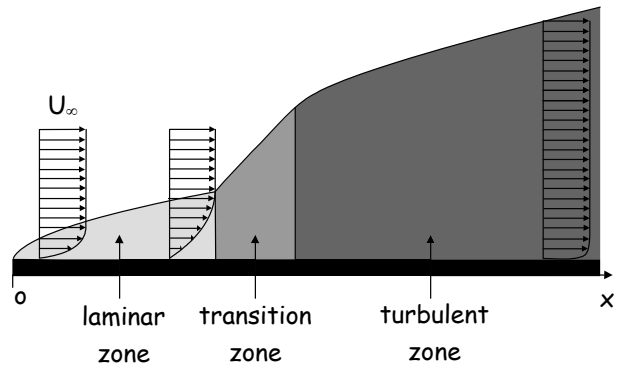


Fig. 9. Transition from laminar to turbulent on a flat plate.

E. Separation

In the case of an airfoil, due to the curvature of the wall an adverse pressure gradient appears. When the pressure gradient becomes positive, then separation takes place. In other words, the velocity gradient perpendicular to the plate decreases and when it becomes null the boundary layer detach the plate. This is the point of separation. Then instabilities appear and a back flow exists, this is the separation zone (figure 10). The existence of such zone on an airfoil induces a lift reduction and an increasing of the drag. This can be easily observed on the experiments made by Prandtl (reported by Schlichting [2]) concerning a flow around a typical airfoil for two different inclinations (figure 10). At small incidence angles (up to about 10°) the flow does not separate on either side (left picture in figure 11). Increasing the incidence the adverse pressure gradient on the upper side of the airfoil becomes larger. For a given incidence angle (about 15°) separation occurs (right picture in figure 11). The separation point is located close behind the leading edge. As a consequence the lift is widely decreased and the drag increased (figure 12). In this figure C_L and C_D represent the lift and the drag coefficients, these two parameters are defined by the following equations:

$$C_L = \frac{L}{1/2\rho U_\infty^2 A} \quad (5)$$

$$C_D = \frac{D}{1/2\rho U_\infty^2 A} \quad (6)$$

Where L is the lift, D the drag, ρ the air density, U_∞ the air stream velocity and A a characteristic area, e.g. the frontal area exposed by the body to the flow direction.

In extreme conditions these consequences may be responsible for airplane stalling and must obviously be avoided, but, even in "normal" conditions, the separation can be important, for instance during takeoff, and induces a very bad efficiency of the airplane. Thus, delaying separation on a wing plane is one of the most important challenges to aeronautics for many years.

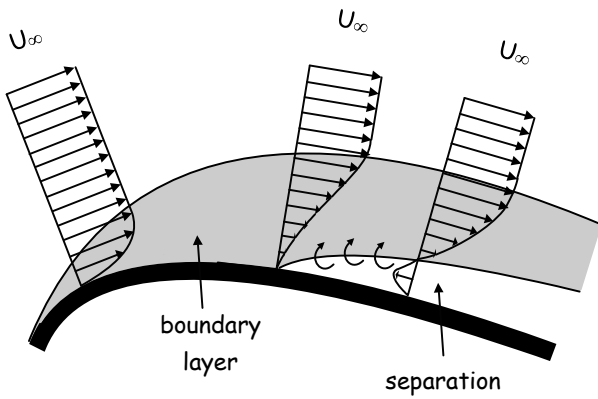


Fig. 10. detachment of the flow.

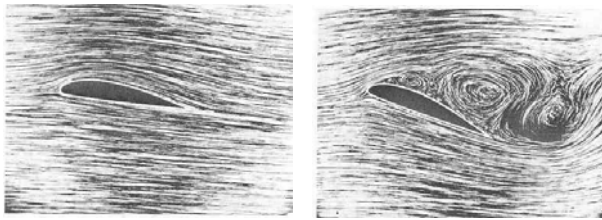


Fig. 11. Experiments showing the dependence of the detachment on the attack angle.

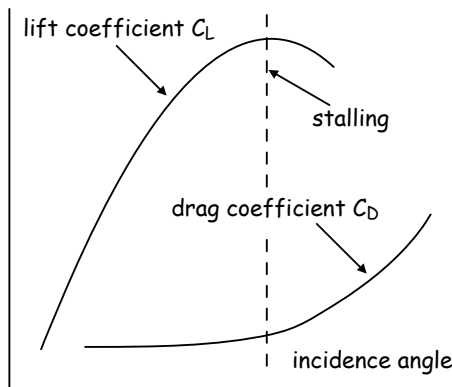


Fig. 12. Evolution of the lift and drag coefficients of an airfoil in terms of the attack angle.

F. Effect of transition laminar to turbulent on separation

One remarkable phenomenon at the transition between laminar to turbulent is the sudden decrease of the drag coefficient. This is for instance the case of spheres or cylinders submitted to a flow (figure 13). At the critical value of the Reynolds number the drag coefficient suddenly decreases and then increases again for larger Reynolds numbers. This surprising phenomenon is in fact due to the transition which causes the point of separation to move downstream, because, in the case of a turbulent boundary layer, the accelerating influence of the external flow extends further in the boundary layer due to turbulent mixing. We can see in figure 14 photographs of

experiments made by Wieselsberger [7] concerning a flow around a sphere. On the left part of the figure the Reynolds number is just below the critical value of transition and the separation occurs before the median plane of the sphere. In the right part of the figure the transition has been induced by a thin wire ring soldered on the sphere before the median plane. The instabilities created by the wire induce the transition to the turbulence, then, as we can see, the separation is delayed. Measurements made with these two configurations show a reduction of the drag coefficient as the figure shows a reduction of the "dead-water area". A practical example of this phenomenon is applied to the golf balls whose surface irregularities allows an earlier transition to turbulence which reduces the drag coefficient and then permit a longer drop of the ball. In summary, the turbulent boundary layers are more negative pressure resistant than the laminar ones. Indeed, momentum transfer by convection is much more efficient than by diffusion. Thus, momentum provided in areas close to the wall where the velocity is very small is much more important in turbulent boundary layers than in laminar ones. In consequence, the boundary layer detachment is delayed.

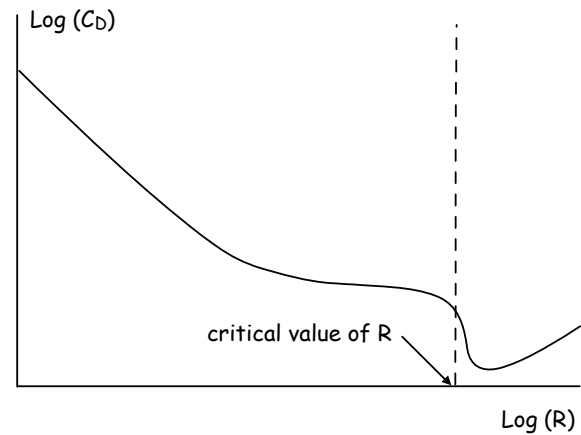


Fig. 13. Sudden decrease of the drag coefficient at the transition laminar to turbulent.

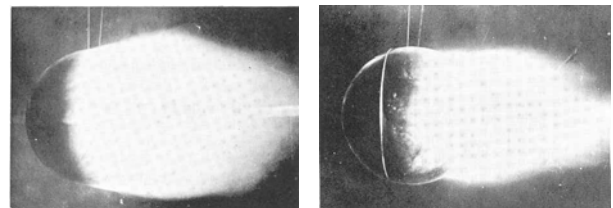


Fig. 14. Experiment of drag coefficient reduction on a sphere at the transition.

In the case of a plane wing, eddies developed in the separation zone generate a transition zone to a turbulent boundary layer as it can be seen in figure 15 for a plane wing with a flap. We can see in this figure that the transition to the turbulence induces a beneficial reattachment of the boundary layer which finally detach only at the beginning of the fowler.

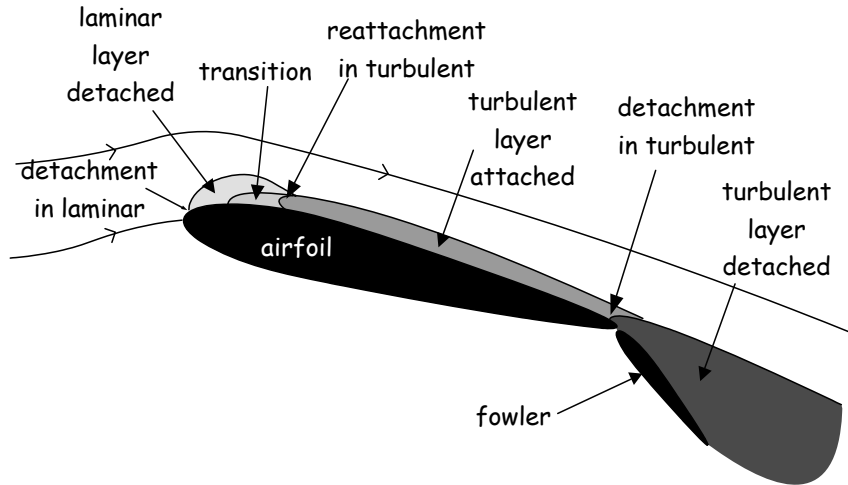


Fig. 15. The different zones around an airplane wing with a fowler.

However, if no separation exists on an airfoil in motion the drag is obviously smaller in laminar than in turbulent, but if the separation occurs it is generally interesting to enhance the transition to turbulence in order to delay the separation, this is one of the techniques used. Anyway, in the case of airfoils like wings or airplane body, delaying the separation will induce a noticeable favorable influence on the efficiency of the airplane. In the next paragraph, we are going to examine the different techniques which have been considered to delay the air flow detachment.

III. AERODYNAMIC FLOW CONTROL

We have seen that drag and lift play an important role in aeronautics and are very closely related to the flow regime and configuration around the different parts of a plane. The goal of flow control is to perform devices or processes which induce the flow configuration and regime wished at a given flight phase of the airplane (takeoff, cruise or landing). Indeed, during these different phases the goal wished may be totally different, more, trying to stay in one regime may induce a configuration worst than that to pass in another regime. For instance, for the same velocity, the drag is smaller for a laminar flow than for a turbulent one, but a laminar boundary layer is very sensitive to the separation process while the turbulent one is more robust, thus, trying to stay in laminar may induce separation which finally gives a higher drag and smaller lift than a turbulent regime. Thus, the action to be taken depends generally on several parameters and is sometimes a compromise.

As Gad-el-Hak in a flow control reference book [8], it is usual to distinguish two kinds of control: passive or active. Passive controls do not use external energy to modify the flow, while active controls use external energy. Passive control devices are generally permanently fixed on the aircraft and cannot be removed, even, they may be a part of the air plane specially designed to control a part of the flow around its body. This is for instance the case of curved end of wing (figure 16). In opposite way, active control devices or

processes may be acting or not depending on the flow configuration. Even if the classification of retractable devices has been sometimes debatable, they will be, following, classified as active control devices because they can be modify in function of the flight condition (takeoff, cruise or landing).

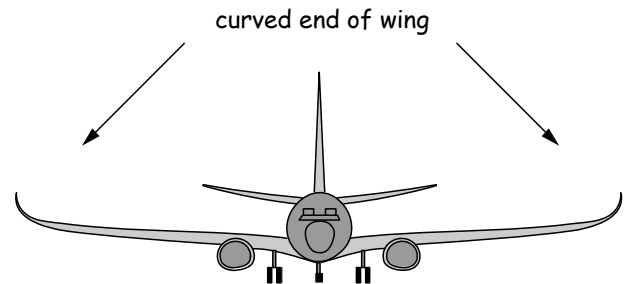


Fig. 16. Example of passive control device.

A. Passive control devices.

Two main devices have been perfected for control in aeronautics, riblets and Large Eddy Breakup devices (LEBU).

Riblets (figure 17) are small grooves aligned with the free air stream. They modify the near-wall structure of the boundary layer. Walsh and al from NASA-Langley laboratory [9] examined the drag reduction for different riblets profiles (figure 18). They found that the best shape seemed to be sharp peak and sharp or round valley. With such riblets profile they found 8% of drag reduction. The size of the riblets (distance between valley and peak) is rather small around 35 μm and can be made on plastic adhesive films stuck on the airfoil. Aircraft manufacturers like Boeing and Airbus have tried such films with 5 to 6% drag reduction.

The purpose of LEBUs [10] is to alter, breakup, or sever the large vortices appearing at the outer edge of the turbulent boundary layer existing around an airfoil. They are usually made of small strips or airfoils (like NACA 0009 in the case of the example shown in

figure 19) placed in the boundary layer. The performance of these devices is generally not better than riblets. The problem encountered is generally the proper drag induces by the LEBUs which finally may not produce a global reduction of the whole drag.

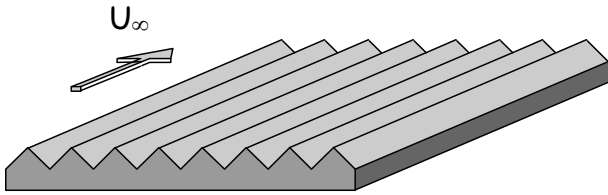


Fig. 17. Airfoil surface with riblets.

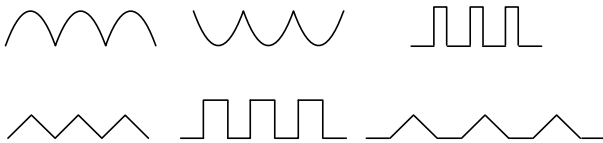


Fig. 18. Different riblets designs.

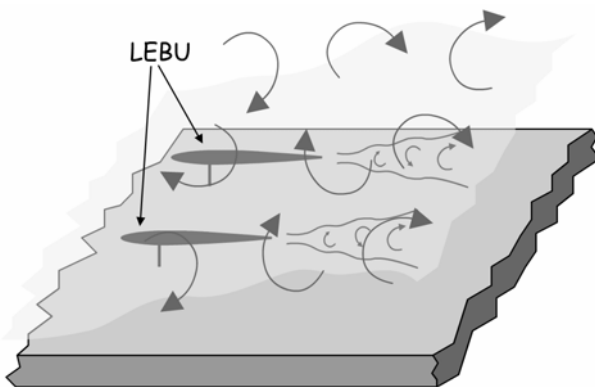


Fig. 19. Example of LEBUs attached to an airfoil.

B. Active control devices or techniques

1) Devices and techniques delaying the separation

In order to avoid the separation three processes can be tried: aspiration, blowing or use of convertible flaps. Aspiration and blowing processes could seem to be contrary but in fact they can both be used in order to delay the separation. Aspiration as we can see in figure 20 in the case of a laminar boundary layer attracts the boundary layer through the plate. This process has been tried in aeronautics. We can see the schema of the process in figure 21. Experiments made on a real plane can be seen in figure 22 (upper picture without actuation and lower picture with actuation) [11].

This process is unhappily difficult to be commonly implemented in aeronautic industry as the small holes of aspiration can very often be closed by particles.

The blowing process (figure 23) increases the velocity very close to the wall in order to delay the null gradient velocity zone which is in fact the beginning of the separation. This process is the most promising for the

manipulation of a laminar boundary layer.

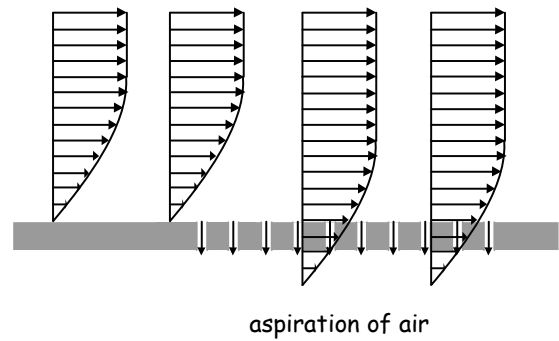


Fig. 20. Aspiration process.

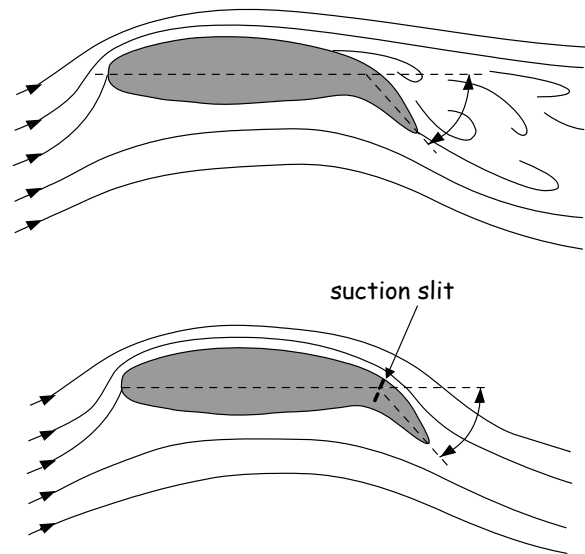


Fig. 21. Schema of suction process on a wing.

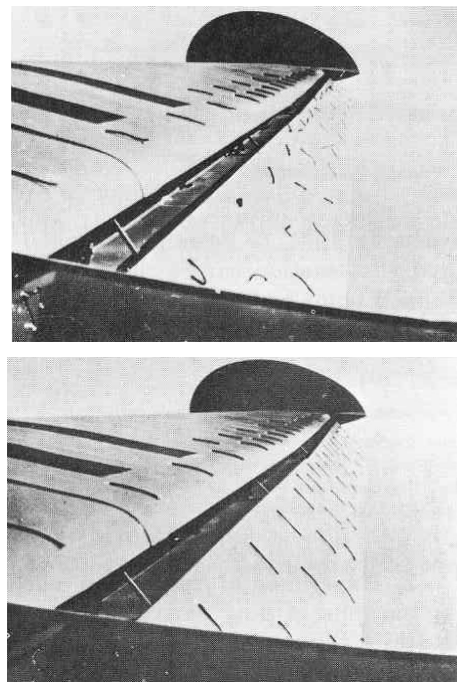


Fig. 22. Suction experiments on a wing.

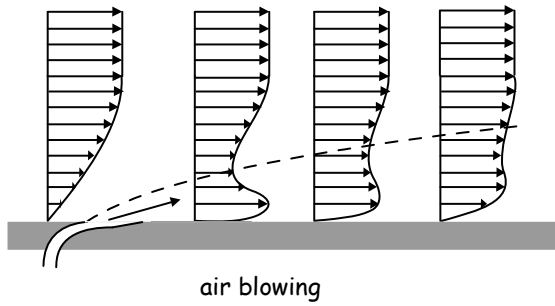


Fig. 23. Blowing process.

2) Forward slots and backward flaps

Retractable slots and flaps are often used on aircraft. They can be used in front of the wing (forward slots or slats) and can have two different purposes, one is to enlarge the wing for a greater lift, the other one is to generate a kind of blowing (figure 24) at the beginning of the wing and thus to delay the separation. An example is the Krueger flap, which is hinged on the leading edge of the wing.

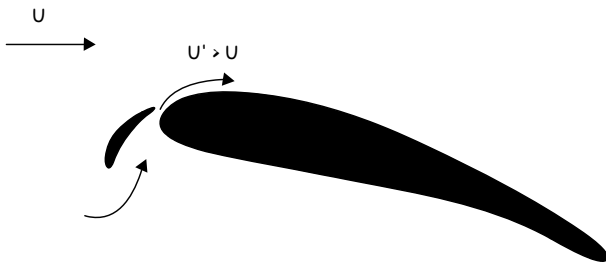


Fig. 24. Forward slots.

Retractable flaps are also used at the rear of wings for the same purposes (Fig. 25).

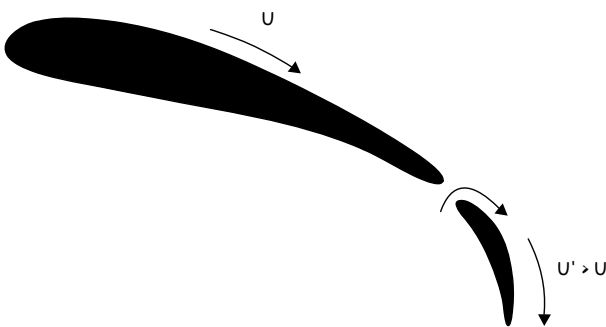


Fig. 25. Retractable flaps.

In fact both are used on commercial planes. They are deployed during takeoff and landing but retracted during cruise (figure 26). The trailing edge flap is also called fowler. However these devices cause an additional drag and this is a disadvantage for takeoff. Generally, flaps are partially extended for takeoff, thus the aircraft has a slower stalling speed but with only a little increase in drag. A slower stalling speed allows the aircraft to take off in a shorter runway distance. Flaps are usually fully extended for landing to give the aircraft a slower stalling

speed so the approach to landing can be flown more slowly, allowing the aircraft to land in a shorter runway distance. The higher drag associated with fully extended flaps allows a steeper approach to the landing site. Thus, for landing even the higher drag is beneficial.

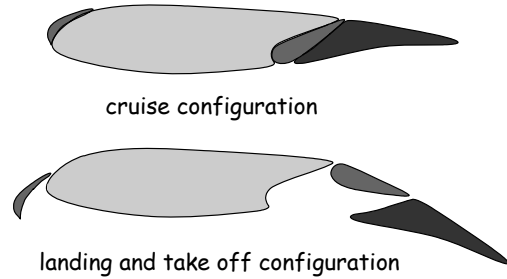


Fig. 26. Slots flaps and fowlers.

Sometimes additional flaps (figure 27), called spoiler are also used during landing operation to reduce the speed of the aircraft.

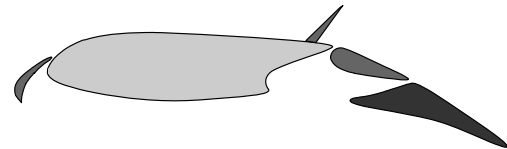


Fig. 27. Spoiler in action

3) Micro-Electro-Mechanical-Systems

Micro electro mechanical Systems (MEMS) have recently been developed in different industrial or medical applications. Due to the high integration capabilities in electronic integrated circuits, it is then possible to gather on the same small scale device a sensor and an actuator. For flow control, micro actuators have been perfected like micro flaps and micro balloons in order to make a control of the roughness of the airfoil (figure 28). In aeronautics, several kinds of micro-jet devices have been perfected. Someone used pulse jets but more attention has been given on synthetic jets. We can see in figure 29 a schema of an example of synthetic jet device. To move these actuators the energy used may be thermo-pneumatic, magnetic, piezoelectric or electrostatic. Low-temperature MEMS are actually under development at NASA Lewis laboratory, with sensors measuring pressure, heat-flux, and strain, directly built on flexible substrates and including interconnects and signal conditioning electronics. This substrate could be then bonded to curved surfaces to enable quick and easy installation and testing.

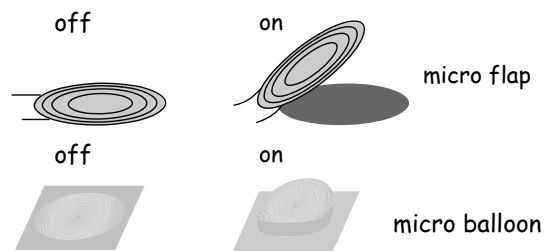


Fig. 28. Example of Micro electro mechanical systems.

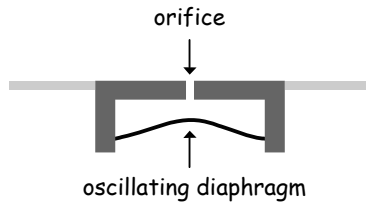


Fig. 29. Synthetic jets MEMS.

C. Summary on flow control devices

Flow control is a very difficult challenge. Indeed, the flow configuration around a body is generally not in a steady state, then, the action need in one configuration may be totally undesirable under other configuration. Thus a predetermined device which in any case makes the same action is often not very interesting. Even, from an aerodynamic point of view, the exact process needed in the boundary layer is often not obvious. However, in aeronautics, two major processes are often needed: to reduce the drag and to avoid the boundary layer separation. But, then the problem is to know exactly what to do to be able to solve such purpose.

We have above seen the different conventional techniques and devices to make airflow control in aeronautics, we are now going to examine the different plasma actuators which have been performed for this purpose.

IV. PLASMA ACTUATORS

After a brief historical summary of electric wind devices, this paragraph will present the different so-called "plasma actuators". The purpose of this overview is not to analyze and compare the efficiency of the different plasma actuators, this has already been made by Moreau in a very exhaustive review [12], the goal here is to describe carefully how the different actuators were made, how they were working, what kind of electric power supply they used, what was the purpose of this special design and operating mode and finally to make a brief comment on the experimental results obtained.

A. Genesis of non thermal plasma actuators.

It is known for a long time that a metallic point submitted to a high electrical potential generates a wind (figure 30 and figure 31).

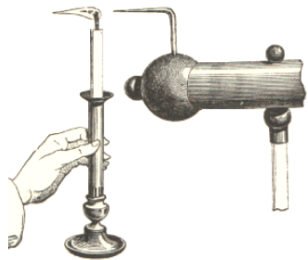


Fig. 30. The candle experiment.

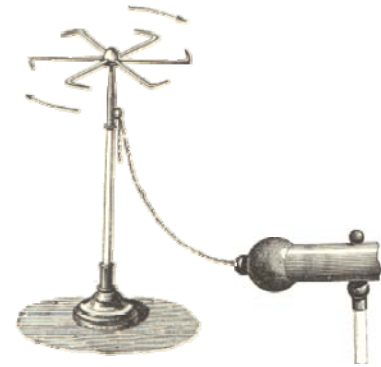


Fig. 31. The turnstile experiment.

The reason is now rather well understood. Near the tip of the point a corona discharge appears, thus ions are created and moved by the electric field. These ions in motion drift the air molecules creating an electric wind (figure 32). This is the basic process of non thermal plasma actuators.

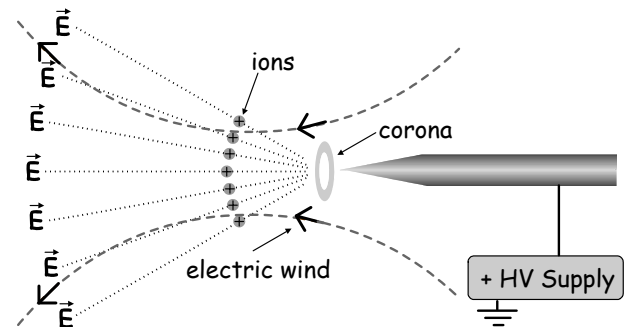


Fig. 32. Electric wind generated at a needle tip.

In the case of actuators to be used in aerodynamic applications, the process is a little more complicated as the actuator must be mounted on the body submitted to the flow and therefore the material of the body induces perturbations as well on the plasma but also on the "electric wind" created, more they need a counter electrode. Nevertheless, the fact that such device has no moving part constitutes a real advantage for use in aeronautic industry.

Plasma actuators may be classified by their geometrical configuration and the kind of high voltage applied. In this paper we are going to examine first the actuators not using a dielectric barrier, then those using a dielectric barrier.

B. Plasma actuators without dielectric barrier

1) Set of wires placed above a flat plate

Velkoff and al in 1968 [13] studied the effect of a corona discharge on the position of the transition in the boundary layer on a flat plate. The flat plate (183 cm long and 91 cm wide) was placed in a wind tunnel whose turbulence intensity was below 0.5%. and the velocity around 53 m/s. The leading edge of the plate was a sharp 15° bevel. They placed above the flat plate four wire

electrodes parallel to the plate 14 mm above the plate and perpendicularly to the flow (figure 33). The four wire electrodes were 0.2 mm in diameter and 15 mm spaced one to the other. This set of electrodes were placed 32.4 cm from the leading edge in the region where the transition laminar to turbulent appeared without applied voltage. Indeed, without wires or even with wires but not connected to the high voltage, the transition occurred at 38.7 cm from the leading edge, while the fourth wire is located 36.9 cm from the leading edge. The four wires were connected to the same high voltage supply. The voltage source had a constant 10 kV component plus an alternative 2 kV component with an adjustable frequency. When the voltage was applied to the wires, electric wind is generated by each wire and the transition was shifted 46 mm downstream (43.3 cm from the leading edge). This phenomenon was independent of the frequency (the same from pure DC to 6 kHz).

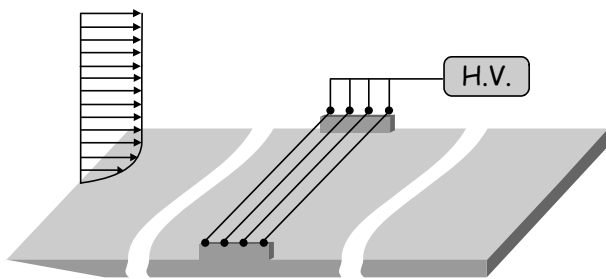


Fig. 33. Experimental setup performed by Velkoff and Ketcham.

2) Flat plate filled with pointing wires

In their experiments, Malik and al [14] used wire brush material (which came in 4 cm wide strip) to perform a flat plate containing metallic needles to produce electrical discharges (figure 34). The wires (0.3 mm in diameter and 6 mm long) were swept back about 30° and the distance between two successive wires was 1 mm. The wire brush material was filled with epoxy resin up to around 0.3 mm from the tip of the wire. The wire was then etched in order to get wire tips of 0.1 mm in diameter. All the wires were electrically connected together by coating the back of the material with conducting paint. The active part of the plate (46 cm long and 19 cm wide) was made with 10 sections of wire brush material bonded together. This active part was mounted in a 61 cm × 23 cm support frame. Due to the wires standing a little out the plate the drag on such plate differed of about 5 to 10 % from the drag on a smooth plate, but the comparison between with and without discharge was made on the same "rough" plate. The counter electrode consisted of 0.1 mm in diameter wires mounted 4 cm above the model in a zig-zag fashion. A DC high voltage was applied between the wire brush material and the counter electrode. Both configurations positive or negative counter electrode were tested. Voltages of up to 20 kV giving currents up to 5 mA were used. The swept points of the wires brush material were tested pointing as well upstream and downstream. The stream velocity in the wind tunnel could vary up to 30 m/s. The boundary layer on the test model was laminar

up to about 5 m/s and turbulent for velocities over 10 m/s. The drag on the entire frame was measured with a drag balance. When the high voltage was turned on some wires of the brush material and the counter electrode glowed visibly in a darkened room. It seemed that only 10 % of the wires of the brush material were glowing, which suggested to the authors that the distance between two successive wires could have been 3 mm instead of 1 mm. Measurements obtained shown a rather large drag reduction for velocity less than 10 m/s but much smaller for turbulent flows (velocity over 10 m/s).

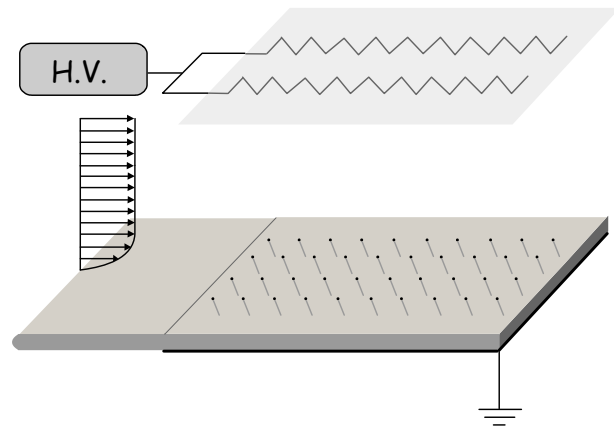


Fig. 34. Experimental setup performed by M.R. Malik and al.

3) Two razor blade electrodes flush mounted against both sides of a flat plate

G.M. Colver and al made one of the first extensive researches on applications of non thermal plasma in air flow control [15-18]. The setup of the experiment is presented in figure 35. It is composed of two blade electrodes flush mounted on the two opposite sides of a flat plate. The plate is placed in a wind tunnel and the drag on the plate is measured without and with a potential difference applied between the two electrodes.

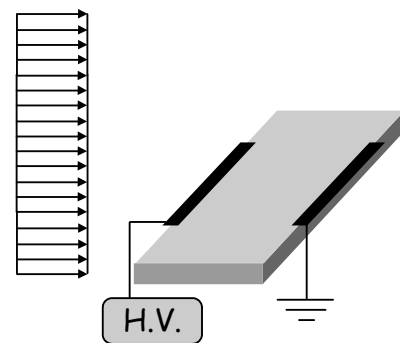


Fig. 35. Experimental setup performed by G.M. Colver and al.

DC and AC voltage differences have been tested. The influence of the voltage difference magnitude and the polarity (in the case of DC voltage) on the drag was analyzed. These experiments were made for relatively low Reynolds number partly for laminar flow. The discharges seemed to be more homogenous in case of AC voltage than for DC, more, they were more homogenous

for positive DC than for negative. They observed a drag reduction up to 73% for a 10 kV AC voltage of 60 Hz frequency. A model has been then proposed [19] for low Reynolds number taking into account the forces due to the electric wind generated between one electrode to the other. The experiments were consistent with the model proposed.

4) *Pointing needle and metallic sheet electrode flush mounted against a cylinder*

In 1996 C. Noger made experiments on the boundary layer perturbations around a cylinder due to corona discharge [20, 21]. A scope of the cylinder and the actuator is presented in figure 36 and figure 37. It is composed of a PMMA cylinder placed in a uniform flow of a small wind tunnel. The upstream side of the cylinder is coated with a metallic electrode grounded, while a needle 6 mm long is placed on the upstream side of the cylinder parallel to the flow and to the cylinder diameter. The high voltage was applied to the needle.

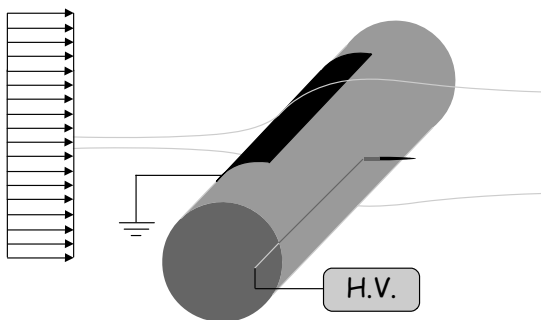


Fig. 36. Experimental setup performed by C. Noger and al (general view).

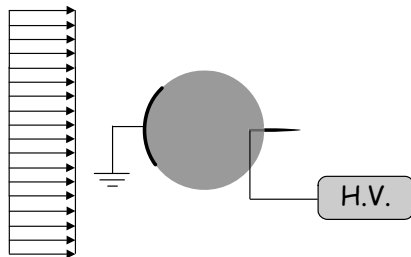


Fig. 37. Experimental setup performed by C. Noger and al (side view).

Experiments were made for low Reynolds number, from 15 to 45. For such Reynolds number it is well known that the flow makes two recirculation bubbles behind the cylinder. The application of the high voltage (up to 7 kV) reduces strongly the size of the recirculation bubbles (up to 80%).

5) *Razor blade electrode on a cylinder*

Later Touchard [22], used the same experimental device than previously described, but with a razor blade instead of the needle (figure 38) and a metallic grid placed far downstream as counter electrode. Experiments gave the same kind of results.

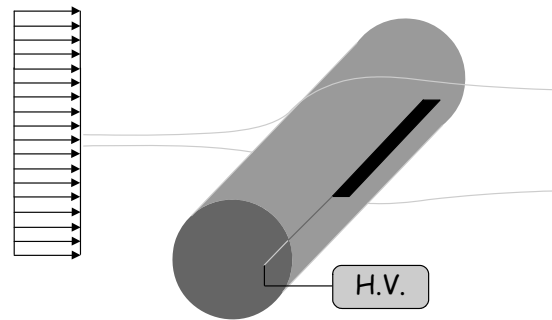


Fig. 38. Experimental setup performed by G. Touchard.

6) *Wire and metallic sheet electrode both flush mounted against a cylinder*

Artana and al made experiments on cylinders also [23, 24]. In these experiments they used a larger wind tunnel and several cylinder diameters. The corona discharge was provided between a thin wire stuck on a cylinder generating line and an aluminum foil stuck on the opposite side of the cylinder. The wire was placed upstream at the stagnation point while the aluminum foil was placed downstream (figure 39 and figure 40). One electrode was connected to a positive DC high voltage supply (0 - 30 kV) while the other was connected to a negative one (0 - 8 kV). Experiments were made for a Reynolds number $Re = 725$ for which the so called Karmans vortex street was clearly apparent for the voltage off, while it was totally destroy when - 8 kV were applied on the aluminum foil and +25 kV were applied to the wire. These experiments and many following were the result of a scientific collaboration between the "Laboratoire d'Etudes Aérodynamiques" of Poitiers University and the "Facultad de Ingeniería" of Buenos Aires in which Moreau and Artana were the main actors [25-29].

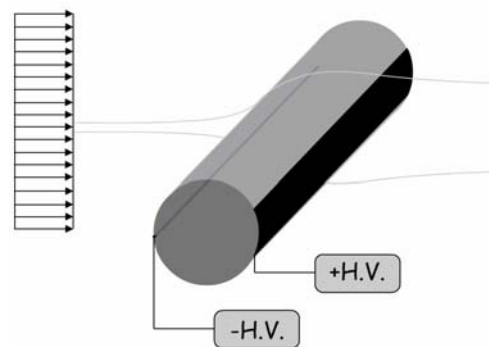


Fig. 39. Experimental setup performed by G. Artana and al (general view).

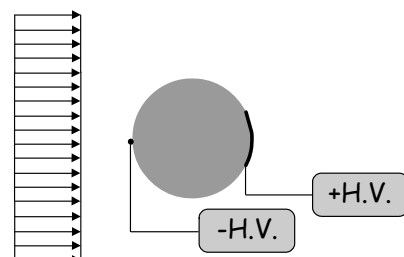


Fig. 40. Experimental setup performed by G. Artana and al (side view).

7) Wire electrode parallel to a conducting cylinder

Hyun and Chun [30] made experiments on a cylinder of diameter 6 cm placed in a wind tunnel with a maximum velocity of 2.5 m/s. A thin aluminum foil covered the cylinder surface and is used as the grounded electrode. Two thin stainless steel wires (diameter 0.09 mm) are both connected to the high voltage supply and placed over and under the horizontal diameter of the cylinder (figure 41). Four different positions are tested (figure 42). In position 1 the two wires are on the vertical diameter line of the cylinder and in positions 3 and 4 downstream the cylinder. Experiments were made for different voltage applied to the wires placed in the different positions and visualization of the flow was recorded. In any wires position, the electric wind generated by the wires had an important effect on the flow pattern.

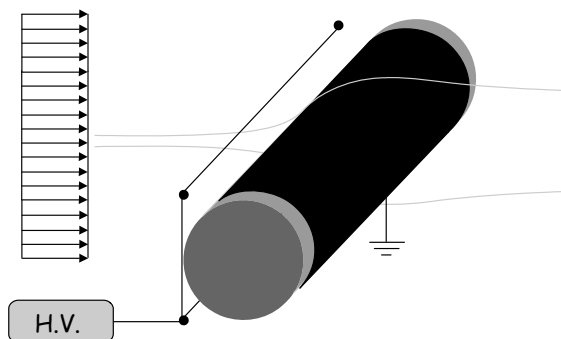


Fig. 41. Experimental setup performed by K.T. Hyun and al (general view).

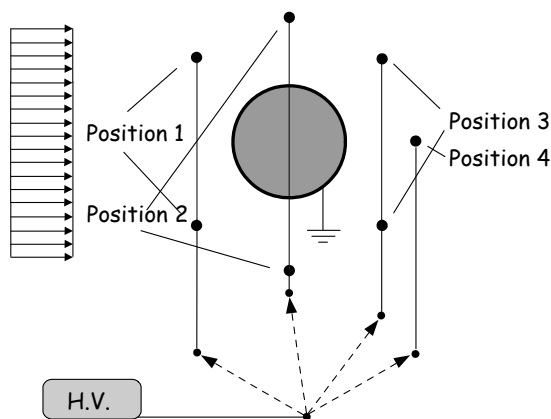


Fig. 42. Experimental setup performed by K.T. Hyun and al (side view).

8) Wire and metallic sheet electrode both flush mounted against an inclined plate

Moreau and Léger made a lot of experiments with this actuator [31-33]. It is composed of a metallic wire, 0.9 mm of diameter stuck at the stagnation point of the plate while an aluminum sheet 25 mm wide is stuck 40 mm downstream from the wire. The plate is 280 mm wide and 150 mm long (figure 43 and figure 44).

The aluminum foil is connected to negative High voltage supply while the wire is connected to a positive one. The potential applied were 18 kV to 20 kV for the

wire and -11 kV to -13 kV for the aluminum foil.

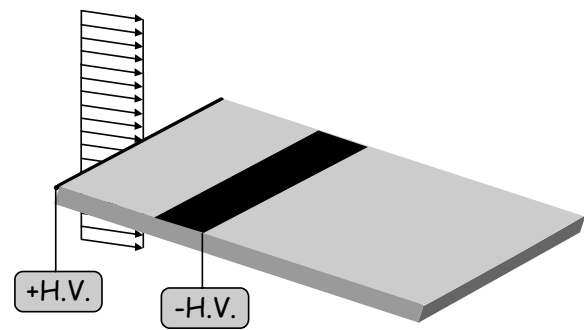


Fig. 43. Experimental setup performed by E. Moreau and al (general view).

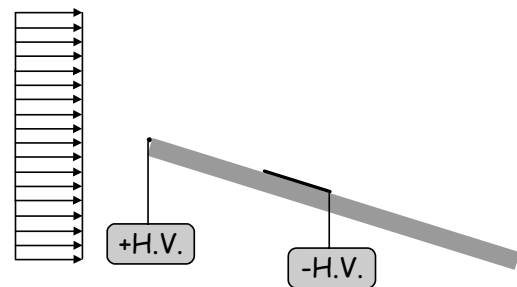


Fig. 44. Experimental setup performed by E. Moreau and al (side view).

Visualizations were made for plate inclination varying from 0° to 50° referred to the stream velocity. The velocity was varying from 0.35 m/s to 1.1 m/s. Without applied voltages, as we have seen in § II A, when the plate is inclined a big eddy developed downstream the stagnation point. When the voltage is applied the flow is reattached up to 30° for the lower velocity and up to 15° for the higher one.

Then, for a flat plate parallel to the stream velocity several other electrode configurations were tested:

- wire stuck on the plate a few cm downstream the leading edge and the aluminum foil 4 cm more downstream,
- same than previously but the wire in a groove
- two wire electrodes, each of them placed in a groove

We are going, following to examine this last configuration which seemed to give the most reliable results.

9) Two wire electrodes inserted in grooves on a flat plate

In this configuration perfected by Léger and al [34] two wire electrodes were inserted in grooves made inside a plastic plate. In order to reduce flow perturbations due to the wire, the size of the grooves were such that the upper surface of the wires were aligned with the plate surface and the width of the grooves fitted perfectly the wires diameter. In a typical configuration which generate a strong electric wind (up to 3.5 m/s), the thinner wire (0.6 mm in diameter) is placed upstream while the wider one (2 mm in diameter) is placed 40 mm downstream

from the other, the thinner wire was connected to a DC high voltage while the bigger one was grounded. Two different flat plates with this actuator have been tested. The first one (figure 45) is a flat plate with a 45° chamfered leading edge and the thinner electrode is placed 7 mm downstream the leading edge.

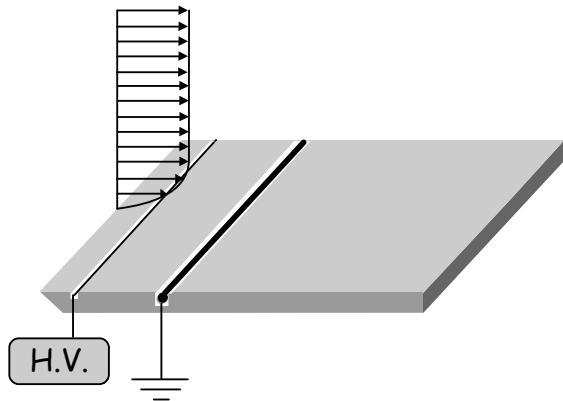


Fig. 45. First experimental setup performed by L. Léger and al

The second one (figure 46) is a flat plate with a rounded leading edge and the thinner electrode is placed 10 cm from the leading edge. For this configuration the electric wind generated had a maximum velocity at about 1 mm above the plate and reach 3.5 m/s for 1.2 mA/m of current density (current by wire length). In fact, the air flow comes from above the anode and not from upstream.

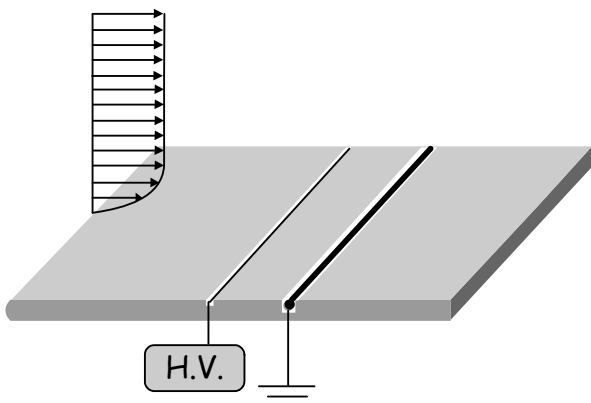


Fig. 46. Second experimental setup performed by L. Léger and al

10) Two aluminum foil electrodes flush mounted on a NACA 0015 profile

Sosa and al performed an actuator placed on a NACA 0015 profile [35-37] made of PMMA. The chord dimension was 200 mm and the wingspan 450 mm. The airfoil profile was placed in a wind tunnel giving a velocity up to 30m/s. The actuator consisted on two aluminum foils flush mounted on the airfoil body (figure47). Each aluminum foil was 15 μm thick and 3.5 mm wide. They covered 85 % of the span and one of them was located at the leading edge while the second one was at 3.6 cm from the first one. The electrode placed on the leading edge was connected to a high voltage

amplifier TREK (0 to ±20 kV, ±20 mA, 20kHz bandwidth) and the other electrode was connected to a DC high voltage supply (-40kV, 3.75 mA). The high voltage amplifier was connected to a function generator. They used square wave starting from 0 V and with a duty cycle of 50%. For an inclination of 19.8° and a 25 m/s flow velocity the boundary layer was totally detached when the actuator was off. Then they put the actuator on. When the maximum voltage on the leading edge electrode was 20 kV with a 50 Hz frequency and -9 kV on the other electrode they observed a boundary layer totally reattached, although power consumed was relatively small, around 5 W.

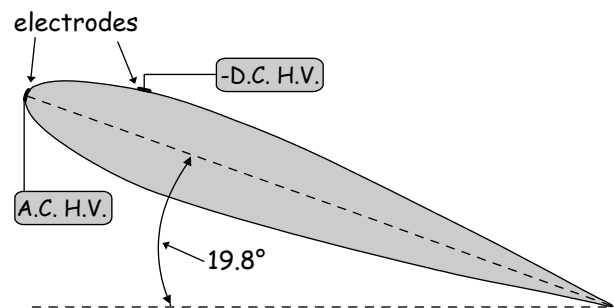


Fig. 47. Experimental setup performed by R. Sosa and al.

C. Three-phase travelling wave actuator

This actuator performed by Moreau and al [38] is composed of several sets of 3 wires flush mounted on a flat plate and connected to three high voltage supplies delivering the same high voltage amplitude but with a phase difference ($\frac{2\pi}{3}$) between one to the next one. The goal was to generate a traveling wave able to drift downstream on a flat plate ions generated upstream. The principle of the setup is shown in figure 48 for only one set of electrodes.

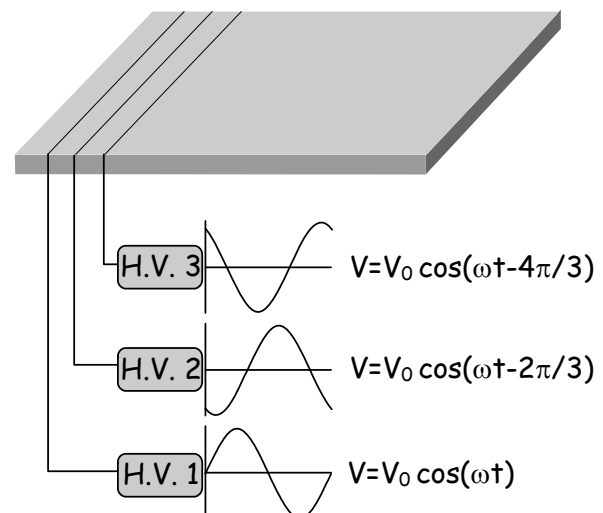


Fig. 48. Experimental setup for three phase traveling waves.

Three different experiments used three sets of wires electrodes (figure 49) (scale drawing). The first one was

made with six bare copper wires 0.7 mm in diameter; the second one used six copper wires of same diameter but covered with a Teflon sheath 1.2 mm in outer diameter; the third one used twelve copper wires 0.25 mm in diameter covered with a PVC sheath 0.6 mm in outer diameter. In the three experiments all the wires were equally spaced on the plate, the distance from one wire to the neighbor was 1 cm for the two first experiments and 0.3 cm for the third one. For the two first experiments using 6 wires, wire No 1 and wire No 4 was connected together to H.V. 1, as well No 2 and No 5 to H.V. 2 and No 3 and No 6 to H.V. 3. For the third experiment using twelve wires, No 1, No 4, No 7, No 10 was connected to H.V 1 ; No 2, No 5, No 8, No 11 was connected to H.V2 ; No 3, No 6, No 9, No 12 was connected to H.V. 3.

	copper \varnothing 0.7 mm	copper \varnothing 0.25 mm
	sheathed with	sheathed with
	Teflon \varnothing 1.2mm	PVC \varnothing 0.6 mm
bare copper		
\varnothing 0.7 mm		



Fig. 49. The different wires used.

Visualizations of flows on this actuator have shown acceleration near the plate and vortex generation behind, but the difficulty was to avoid back flow when a wire voltage was higher than its upstream neighbor voltage.

Generally speaking, actuators without dielectric barrier have several disadvantages: DC discharges are sometimes unstable and very sensitive to humidity.

D. Plasma actuators using a dielectric barrier

1) Dielectric Barrier Discharge (DBD) actuator

DBD actuators used generally two metallic foils flush mounted on each side of an insulating material (figure 50 and 51). Alternative high voltage is applied between the two electrodes, generating a plasma sheet at each facing edge of the electrodes. Sometimes the lower grounded electrode is embedded in the insulating material in order to avoid electric wind generated under the plate (figure 52).

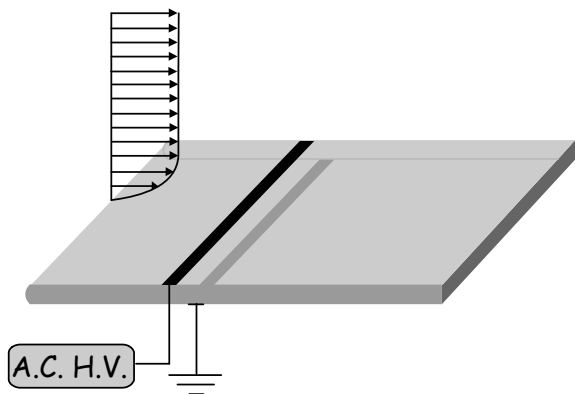


Fig. 50. DBD actuator (general view).

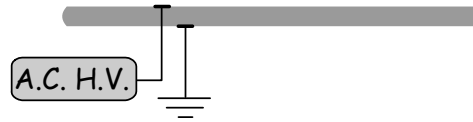


Fig. 51. DBD actuator (side view).

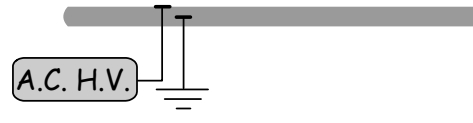


Fig. 52. DBD actuator with grounded electrode embedded (side view).

This actuator produces electric wind whose configuration and magnitude are similar to those of the DC actuator but is more stable and much less sensitive to the humidity. Parametric studies have been made in order to optimize this actuator [39-42] in terms of electric wind velocity.

Concerning the geometry of the actuator (figure 53), it is shown that the distance "d" between the two electrodes must be rather small, 0 to 5 mm, the material thickness "e" must not be too small to have a good stability, 2 - 3 mm seems to be convenient, the optimized width of the grounded electrode "l" is equal to the plasma sheet width which depends on voltage amplitude and frequency. The dielectric constant play also a role, the electric wind velocity generated increases with the dielectric constant. Concerning the electrical parameters, the velocity increases with the voltage amplitude and the frequency but reaches asymptotic values.

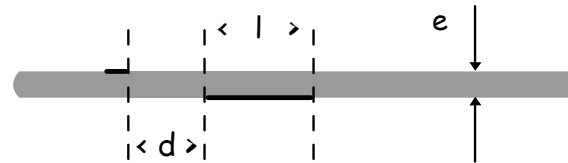


Fig. 53. The different geometrical parameters of a DBD actuator.

2) Sliding discharge actuator

For aerodynamic applications, this actuator has been perfected for the large plasma zone that it can generate. Indeed, with a DBD actuator growing the voltage or sometimes the frequency enlarges the plasma zone and, at the same time, increases the electric wind velocity. Thus, one can expect that bigger the plasma zone is and greater is the electric wind generated. It is composed of three electrodes, generally made of metallic foils flush mounted on the dielectric plate (figure 54 and figure 55). The upper left electrode and the lower electrode furnish a DBD whose the plasma zone can be under certain conditions enlarged toward the upper right electrode [43].

In a typical configuration, the upper left electrode is connected to a DC+AC power supplies; this means that the potential applied to this electrode has two components: an alternative one added to a constant one. It is in fact a periodic voltage which has a non null time-

averaged value. The lower electrode and the upper right electrode are connected together and grounded.

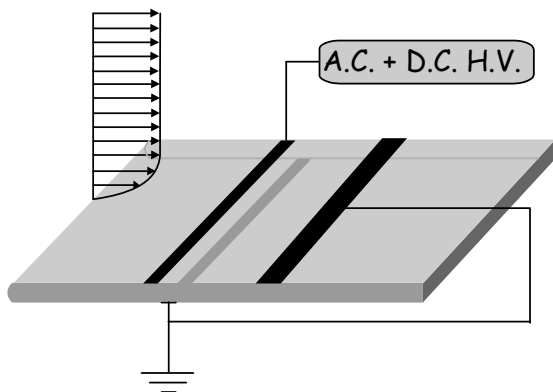


Fig. 54. Sliding actuator (general view).

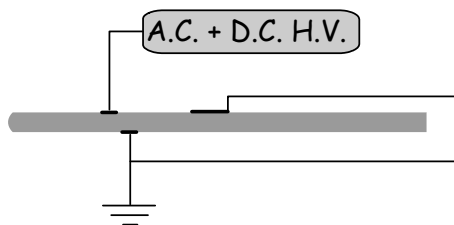


Fig. 55. Sliding actuator (side view).

Typically the AC voltage amplitude applied is between 5 kV and 20 kV with a sinusoidal waveform, the frequency is several hundreds Hertz to 1kHz and the DC voltage amplitude is between 5 kV and 15 kV. Some times only an alternative (AC) potential is applied to the upper left electrode while a DC voltage is applied to the set composed by the upper right electrode and the lower electrode. In both configurations the results obtained are similar. The width of the plasma zone generated with this actuator can easily reach several cm, but the electric wind is in the same order than with the DBD actuator.

3) The One Atmosphere Uniform Glow Discharge Plasma (OAUGDP)

This actuator has been perfected and patented by the group of Roth [44, 45]. It is based on sets of parallel DBD actuators. Experiments have been made on a flat plate in the NASA Langley 7x11-inch Low-Speed Wind Tunnel. The dielectric material used was conventional dielectric printed circuit board material (woven-glass/epoxy construction, 0.75mm thick), it was copper coated and the actuator electrodes were obtained as usual tracks are made on printed circuit board. The dielectric panels (3 were tested having different electrodes configurations) were nearly square (270 x 273 mm).

The upper side (in contact with the air of the wind tunnel) contained 26 copper strip electrodes. The three different electrodes configurations corresponding to the three different panels tested are shown in figure 56 (figure on scale). In all case electrodes are regularly staggered. In figure (56 a) the electrodes are 2 mm wide

and 8 mm spaced (center-to-center electrodes), this configuration is called symmetric because the lower side electrodes are placed at the middle of two upper side electrodes. In figure (56 b) the electrodes are 0.5 mm wide and 8.5 mm spaced, this configuration is called asymmetric because the lower side electrodes have one side just below the opposite side of the corresponding upper side electrode. In figure (56 c) the electrodes are 0.5 mm wide and 10.5 mm spaced, this configuration is called planar because the lower electrode is a planar copper sheet covering all the dielectric. For wind tunnel tests the panel was attached with double-side adhesive tape to a 12.7 mm thick fiber glass backing board in order to make it structurally rigid.

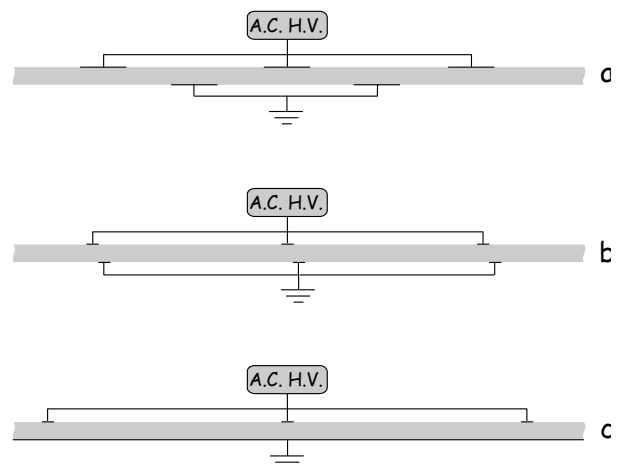


Fig. 56. Configurations of electrodes.

Using the configuration presented in figure (56 a), (symmetric electrodes) two orientations of the panel have been tested, electrodes parallel to the mean airflow velocity (called streamwise) (figure 57) and electrodes perpendicular to the mean airflow velocity (called spanwise) (figure 58).

In both cases, the 26 upper side electrodes were connected to the high power supply delivering voltage up to 5.4 kV with a frequency up to 20 kHz. Drag measurements, in terms of wind tunnel air stream velocity (from 1.5 m/s to 26 m/s), made for 4 kV and 3 kHz, showed an increasing of drag for the actuator on with a slope comparable to the slope obtained with a turbulent flow, when for actuator off the transition laminar/turbulent occurred around 7-8 m/s.

The higher advantage of these actuators was not so the magnitude of the electric wind generated, which was in the order of a few m/s, but their ability to enhance the transition from laminar to turbulent. Other arrangements have been proposed by Roth [45]. We can see in figure 59 actuators in which all the electrodes are embedded inside the dielectric material.

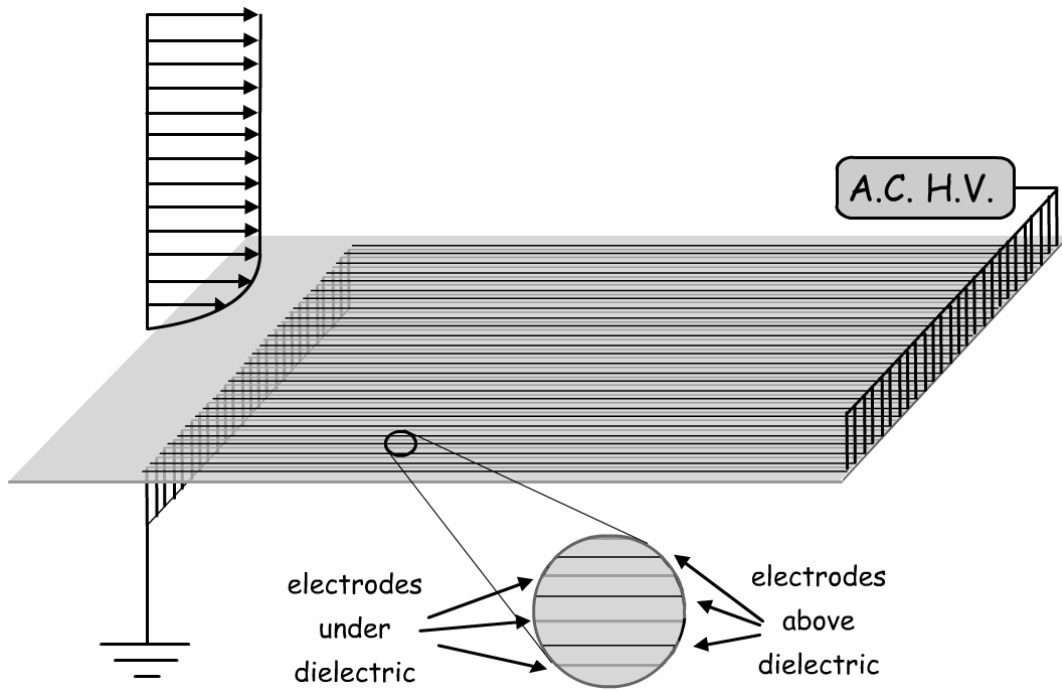


Fig. 57. Streamwise orientation.

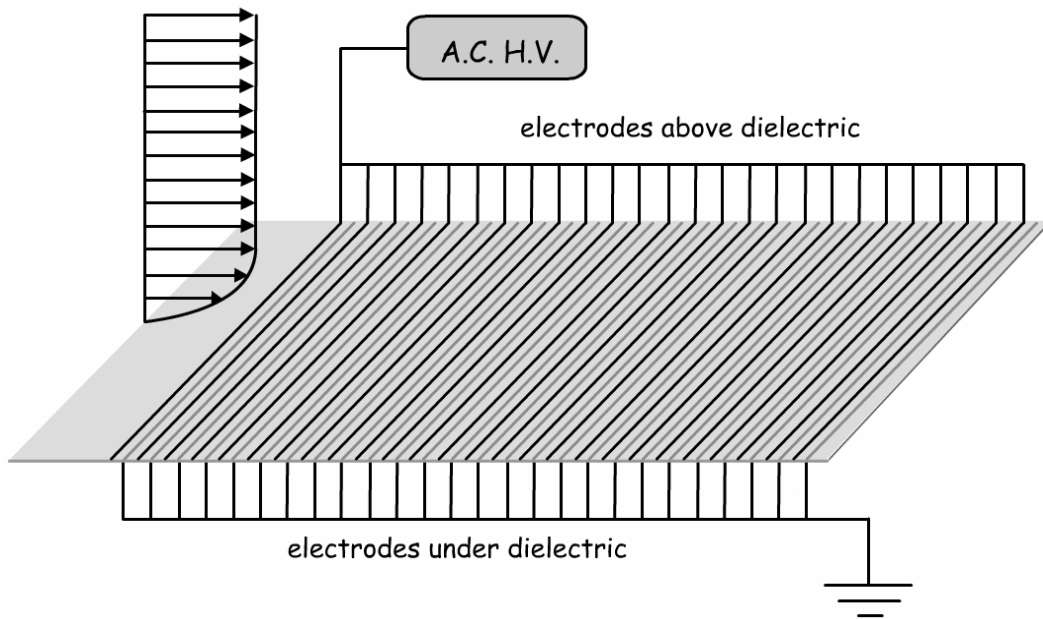


Fig. 58. Spanwise orientation.

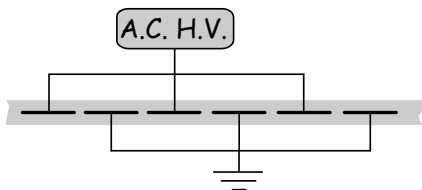


Fig. 59. Configuration with all electrodes embedded.

In figure 60, two arrangements are shown in which multiphase high voltage electrodes are proposed. The panel was 25 x 25 cm and contained 25 upper side strip

electrodes separated by 1 cm and one lower side planar electrode or lower side symmetric electrodes. Experiments were made with 3 sets of upper electrodes. Each set is composed of 8 electrodes with a 45° phase difference between two successive electrodes. With a frequency of 3.3 kHz and a voltage of 4.5 kV it was shown that the electric wind produced on the upper side of the panel was perpendicular to the electrode and in opposite direction for $\Phi = \frac{\pi}{4}$ than for $\Phi = -\frac{\pi}{4}$. A schema of the panel with 24 electrodes reported by J.R. Roth [46] is shown in figure 61.

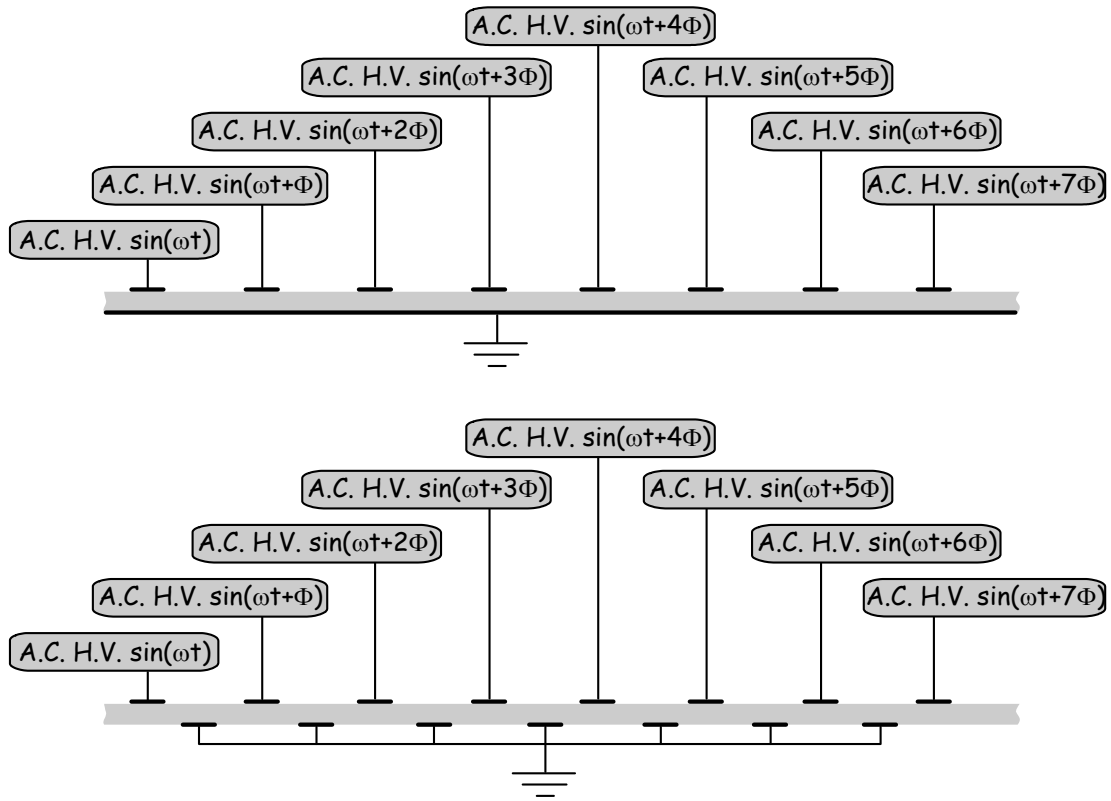


Fig. 60. Side view of eight phases traveling wave arrangements.

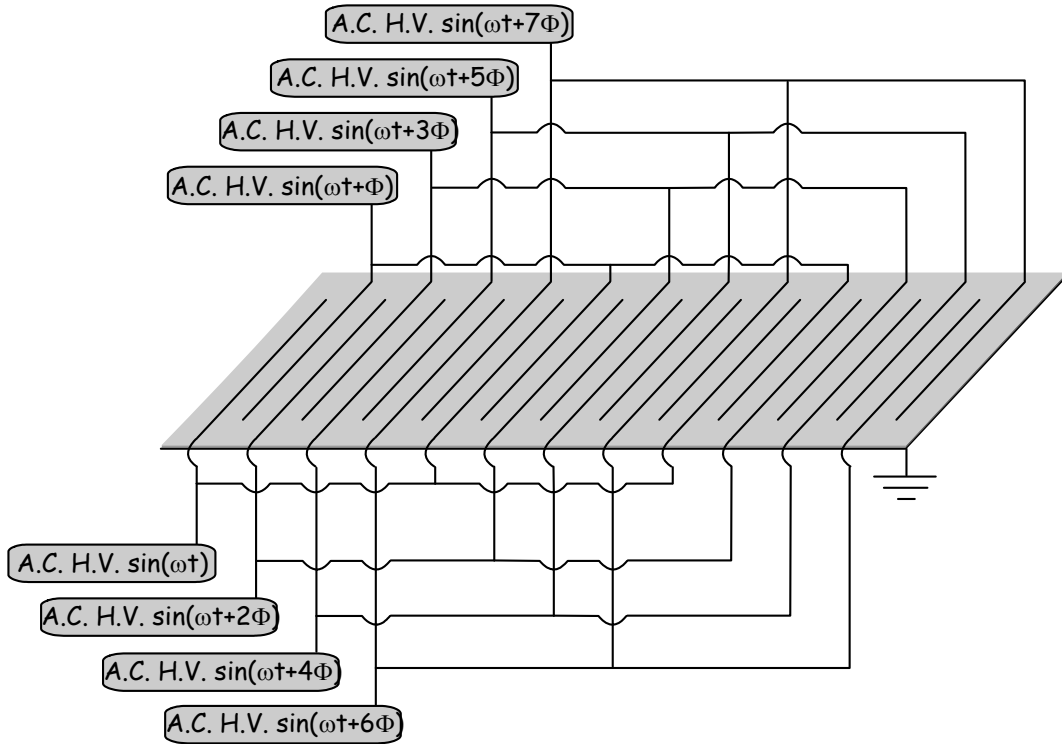


Fig. 61. General view of one realization of eight phases traveling wave device.

Roth has also tested the configuration shown in figure 56 b (asymmetric configuration) on a NACA 0015 profile with 8 pairs of electrodes (figure 62). The flexible panel containing the electrodes was mounted on the airfoil. The

chord of the airfoil was 12.7 cm long. The electrodes were connected to a power supply providing 4.2 kV rms and 4.2 kHz. With this configuration a reattachment was induced by the actuators at 12° of attack angle and 2.85

m/s air flow velocity, but the flow remained detached at 16° of attack angle.

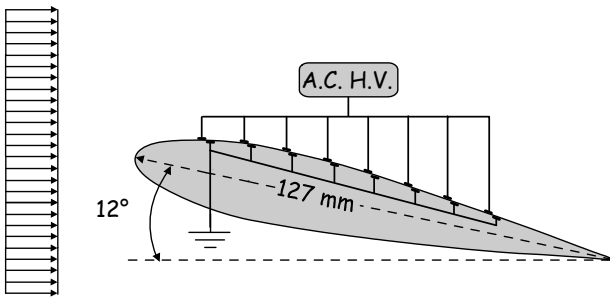


Fig. 62. OAUGDP with eight actuators on a NACA 0015 airfoil.

4) Slat and flap as DBD actuators

One of the most active groups in the field of non thermal plasma actuator for aeronautic applications is the group of T.C. Corke. They generally used DBD actuator on NACA profiles. As a rather recent example [47] of arrangement that they have used, we can see in figure 63 a NACA 0015 profile experimented with two DBD actuators performed to reproduce the effects of a leading edge slat and a trailing edge flap on an airplane wing. Indeed, we have seen in § III.B.2, that the most common used devices on aircraft are slats, flaps and spoiler, the problem of such devices is that important, complex and heavy mechanisms are associated to them, to deploy and retract them, more they operate very slowly. Thus, replace these heavy devices by plasma actuator is an exciting goal. In the example above cited, T.C. Corke and his group made experiments on a NACA 0015 airfoil which had a 12.7 cm chord and a 30.48 cm span. Experiments were conducted in a wind tunnel for two air stream velocities: 21m/s and 30m/s. As they analyzed the changes in drag and lift on the airfoil, the airfoil was mounted on the support sting of a lift-drag force balance.

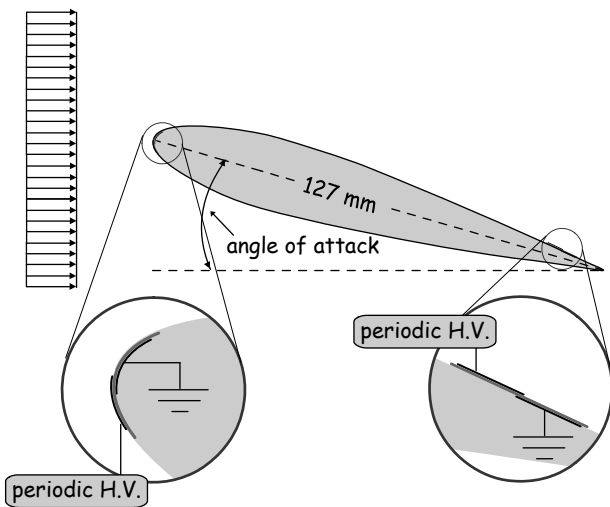


Fig. 63. Leading edge and trailing edge actuators.

They used DBD actuators made of two copper electrodes separated by two Kapton film layers (0.1 mm thick each of them). The electrodes were made with foil

copper 0.0254 mm thick. A little overlap of 1 mm between these electrodes was set to ensure uniform plasma all along the electrodes (in the spanwise direction). The upstream electrode was stuck on the upper side of the dielectric (in contact with the airflow), while the downstream one was stuck on the lower side (figure 64).

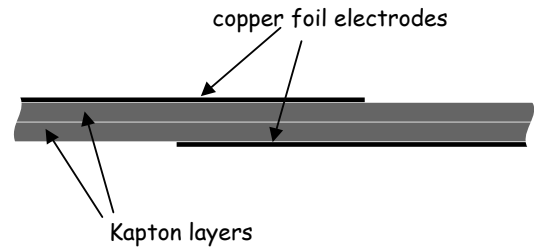


Fig. 64. The actuator configuration.

Thus, with such arrangement, the actuators induced an electric wind velocity in the air stream direction. The actuators were directly bonded to the surface of the airfoil. The upstream actuator was placed exactly at the leading edge (0% of the cord), while the downstream one was placed near the trailing edge (90% of the cord). A special care was taken concerning the leading edge actuator in order to avoid any modification of the nose radius, thus, a special recess (0.1mm thick) was molded in the airfoil profile to ensure no change in the NACA profile. Experiments were made separately for the two actuators. The High voltage amplitude was from 7 to 11 kV peak to peak, the frequency used was between 3 and 5 kHz. In fact, two kinds of actuation was used, one call the steady one used directly the frequency of the source, the other one, called "unsteady" used the sinusoidal signal modulated by a square wave signal whose duty cycle could be adjusted (figure 65). The frequency of the square wave envelope was obviously much smaller than the frequency of the high voltage source.

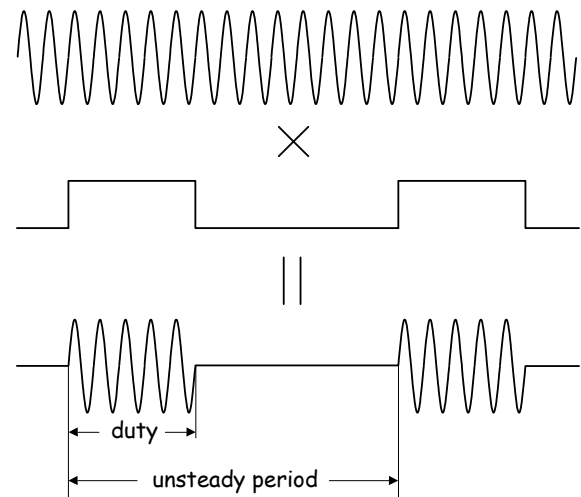


Fig. 65. High voltage modulation.

Experiments using the leading edge actuator showed reattachment up to 19° angle of attack while normally flow separates around 14° , this for two air stream velocities (21m/s and 30m/s). Another important result is that, using unsteady actuation, the optimum unsteady

frequency for reattachment (that is to say the unsteady frequency for a minimum voltage applied) is, as it is usually expected for unsteady disturbances, close to the ratio of the free air stream velocity by the chord of the airfoil (a frequency corresponding to a Strouhal number equal to unity).

Experiments using the trailing edge actuator with a 21 m/s free air stream velocity showed a ratio lift over drag enhanced by a factor of 2.8 to 2 for steady actuation in the range of 15° to 20° angle of attack and 2.7 to 2 for unsteady actuation in the range 15° to 18° angle of attack.

5) Pulse DBD actuators

Recently experiments have been performed on a NACA 0015 profile by the group of Starikovskii [48] using a set of DBD actuators (3 successive) supplied with a pulse generator. The chord length of the profile was 9 cm. The thickness of the dielectric (fluoroplastic) was 0.5mm and the frequency used was 6 kHz (figure 66). It seems that they succeeded to reattach for a 21° angle of attack and 75m/s airflow velocity.

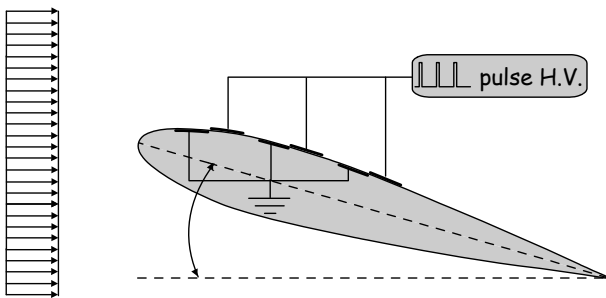


Fig. 66. Three pulse DBD actuators on a NACA 0015 airfoil.

6) DBD actuators on a cylinder

Experiments have been made by Thomas and al on a quartz glass cylinder 100 mm in outer diameter and around 60 cm long [49]. The wall thickness of the cylinder was 2.5 mm. Two symmetric pairs of actuators were used, one pair was located on radii doing 90° with the free air stream direction; the other one was located on radii doing 135° with the free air stream direction (figure 67).

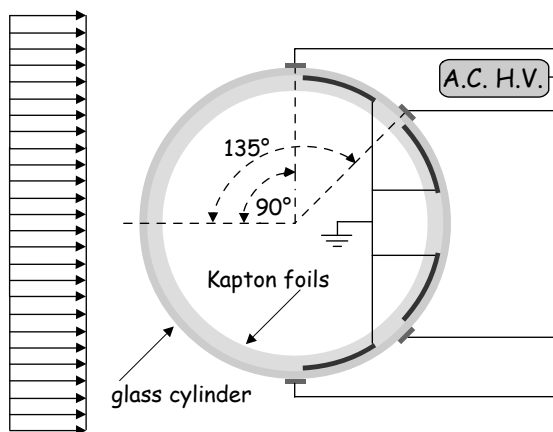


Fig. 67. Side view of 2 DBD actuators on a cylinder.

The outer electrodes were made of 0.04 mm thick copper foil tape and were 6.4 mm wide; they were stuck on the outer part of the cylinder. The inner electrodes were made of 0.04 mm thick lead foil tape and were 25.4 mm wide; they were stuck on the inner part of the cylinder. All the electrodes were around 50 cm long. Seven layer of 0.13 mm thick Kapton foil tape covered the inner electrodes. A small overlap was made between inner and outer electrodes. The outer electrodes were connected to a high voltage AC source providing 8.1 kV rms of sinusoidal form with a frequency of 10 kHz. The inner electrodes were grounded. Two kinds of actuations were done, steady and unsteady, in a similar way that those presented in § IV.D.4. Smoke flow visualization experiments were made for $Re_D=33000$ (free air stream velocity around 5 m/s). For such velocity the effect of the actuators is clearly noticeable, the separated flow region is substantially reduced and the associated vortex shedding appeared to be virtually eliminated. With unsteady actuation it was found that the optimum unsteady frequency was 48 Hz. A duty cycle of only 25% still gave an important reduction of the near wake behind the cylinder.

7) DBD actuators performing oscillating flows

It has been shown [50] that oscillating flows in the spanwise direction (perpendicular direction of the mean air stream) on an air plane wing could be an effective technique in turbulent boundary layer control. The two following actuators were performed in order to reach this goal.

a) Three AC voltages DBD actuators with same amplitude but different frequencies

Two arrangements have been tested by Wilkinson [51], they are made of one or two (figure 68 and figure 69) sets of DBD actuators. These arrangements were performed in order to produce oscillating flow for turbulent drag reduction. Each set was composed of one upper electrode made of 0.1 mm thick aluminum tape stuck on the upper side of a 0.75 mm thick epoxy-woven glass printed circuit board and two electrodes made of the same aluminum tape and stuck on the lower side of the printed circuit board. The lower electrodes were encapsulated between the printed circuit and a 1.2 mm thick float glass glued to the printed circuit with epoxy adhesive. The two lower electrodes were separated by a distance equal to the width of the upper electrode just located between the two lower ones. A reasonable distance separates the two sets.

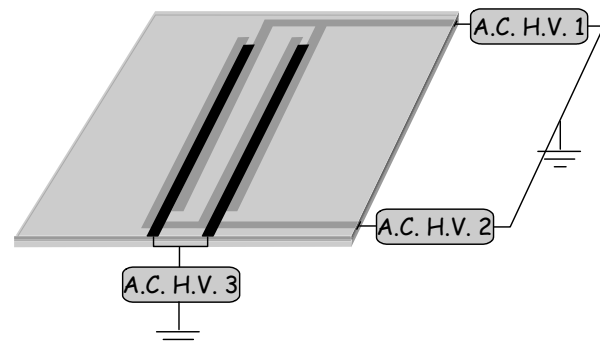


Fig. 68. General view of the setup with two sets of DBD actuators.

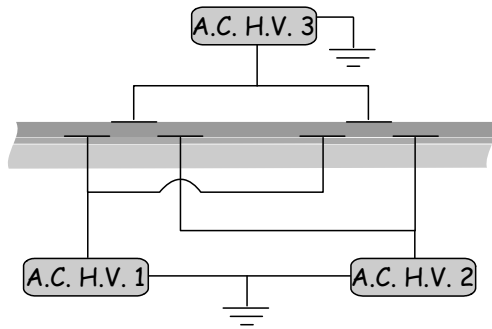


Fig. 69. Side view of the actuators.

The two lower electrodes were connected to two different AC sources which amplitude was the same (around 3 kV rms) but having different frequencies. The upper electrode was connected to another high voltage source whose amplitude was the same than the two other sources but whose frequency was different. The goal of such device was to perform an oscillating flow. In fact, even if small oscillating flows could be obtained for some frequencies, the effect was lost for low frequency (< 100Hz); furthermore, a mean flow was also generated at the same time and complicated the effect.

b) Two alternately energized sets of DBD actuators.

This arrangement tested by Jukes [52] was performed in order to reduce turbulent drag by spanwise (in direction perpendicular to the free air stream velocity) flow oscillation. The actuators panel was manufactured from a 250 μm thick Mylar sheet coated with 17 μm thick copper on both sides. Then the copper is photochemically etched to make the electrodes. We see in figure 70 a part of the Mylar sheet with 5 set of electrodes. On the upper side (in contact with the air stream) two set of electrodes were etched. On the lower side one set of larger electrodes was etched. A side view of a part of the setup is presented in figure 71. Experiments have been made for several distances between the lower electrodes which was greater than the lower electrodes width, a typical value of this distance was 4 mm.

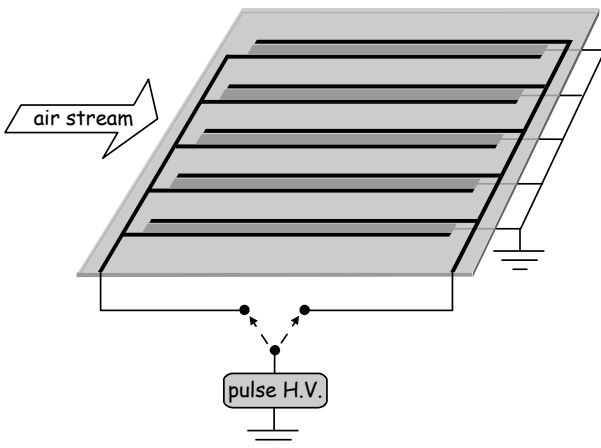


Fig. 70. General view of the setup.

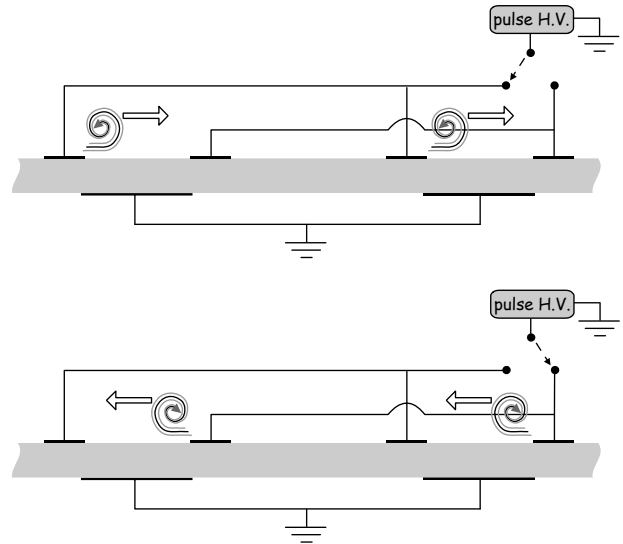


Fig. 71. Side view of the setup for two different voltage connections.

Each set of the upper electrodes was alternately connected to the pulse high voltage supply, while the lower electrodes were grounded. The high voltage applied to the upper electrodes was in the form of alternating polarity pulses, around 4 kV in amplitude and had variable duration and frequency. A typical duration pulse was 10 μs, while, what they called the Pulse Repetition Frequency (PRF), was typically 50 kHz (this means that the pulse duration was equal to the zero potential duration). A set of successive alternating polarity pulses composed a train of pulses. The duration of a typical pulses train (they called it Pulse Envelope Duration PED) was typically 5 ms. Frequency of channel switching (what they called the Pulse Envelope Frequency PEF) was typically 20 Hz. In such configuration the duty cycle for the train of pulses was 10%, however the two parameters PED and PEF was controllable. We can see in figure 72 these different parameters.

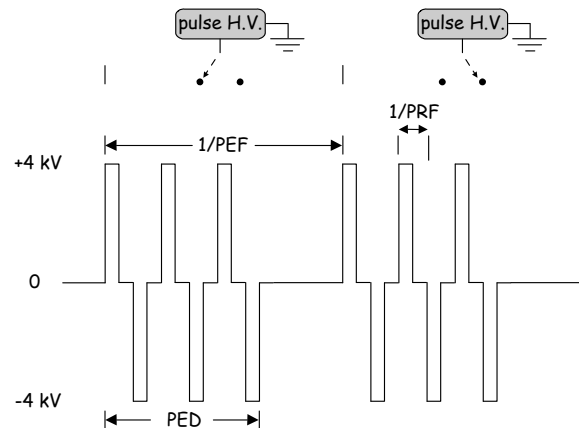


Fig. 72. Pulses configuration.

The goal was reached as alternately flow was generated in the near wall region with alternately clockwise and counter-clockwise vortices as it is shown in figure 71.

8) DBD actuators performing a jet

a) Annular plasma synthetic jet actuator

One actuator has been performed by Santhanakrishnan and al [53] to produce an annular synthetic jet or suction. A typical arrangement performed (figure 73 and 74) consisted of a 0.6 mm thick alumina ceramic sheet and one copper electrode on each side. The alumina ceramic was used as dielectric barrier. One electrode was annular 25.4 mm in outer diameter, the other electrode was circular 12.7 mm in diameter. The center of each electrode was common (axially symmetric device). The inner diameter of the annular electrode was either equal to the diameter of the circular electrode or 1 to 2 mm smaller in order to have 1 to 2 mm of overlap. The upper electrode was in contact with air while the lower one was embedded (all the setup above describe was placed over a layer of non-conductive material, such as acrylic or P.M.M.A.).

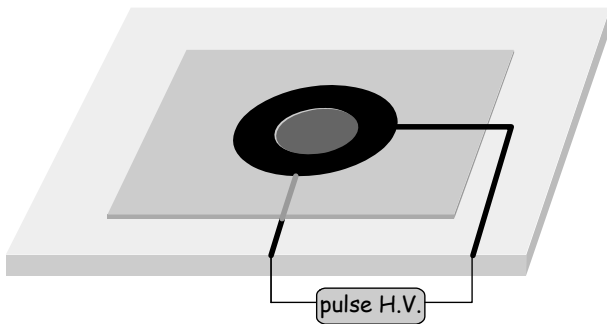


Fig. 73. General view of the actuator.

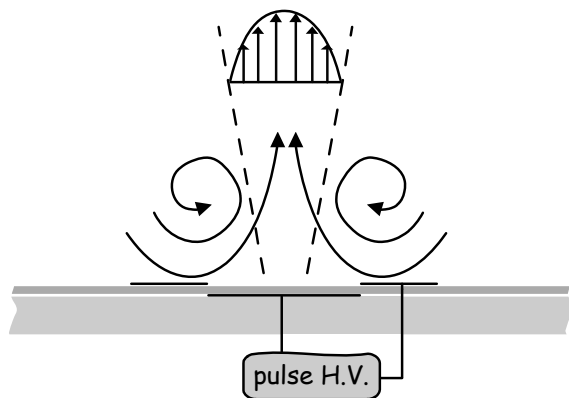


Fig. 74. Side view of the actuator.

The high voltage was obtained with a function generator connected to a power supply itself connected to the input of a non-inductively matched step-up transformer whose output is sent to the electrodes. Typically, the high voltage pulses were 5 kV in amplitude, 2.8 kHz in frequency of square waves with 50% duty cycle (figure 75). The electrodes were energized by the high voltage at different frequencies (1Hz, 10 Hz, 100 Hz) called pulsing frequency (f_p) and also constantly. This actuator could perform jets up to around 1 m/s.

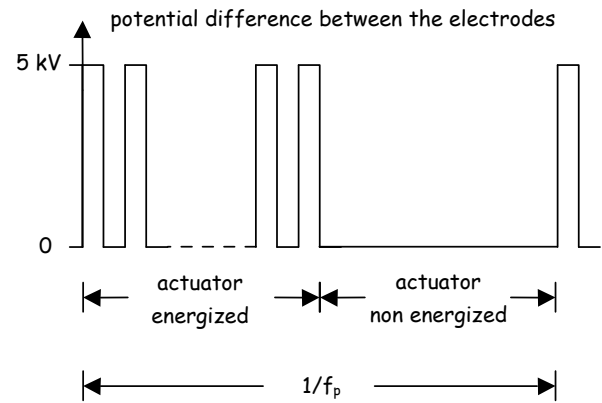


Fig. 75. High voltage pulses configuration..

b) Bi-dimensional directional jet actuator

A bi-dimensional jet actuator has been performed by Bénard and al [54]. The originality of this device was the possibility to orient the jet produced. It was composed of two DBD actuators connected to two AC High Voltage power supplies working simultaneously (figure 76). The two lower electrodes (under the plate) were grounded while the two upper electrodes were connected to two power supplies synchronized. The electrodes were made of aluminum foils (20-mm-large and 200-mm-long). The two lower electrodes were separated by 3 mm in order to measure the current on each one. The two upper electrodes were separated by 43 mm. Thus, between the edge of each upper electrode and the edge of the corresponding lower electrode no gap existed. The plate was 3 mm thick and made of PMMA.

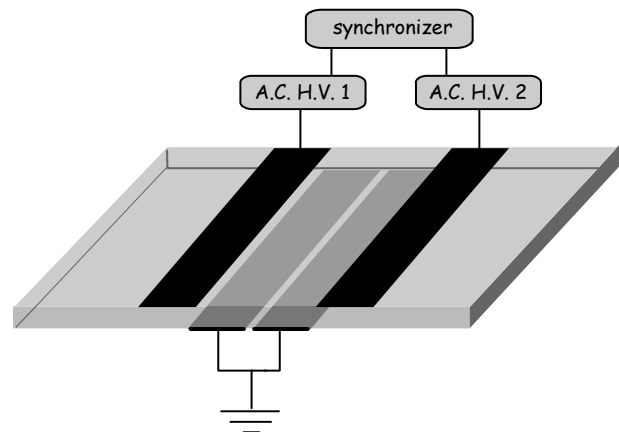


Fig. 76. General view of the actuators.

We can see in figure 77 a diagram of the electrical circuit. The two high voltages were given by two different high voltage amplifiers. These two amplifiers were supplied by two function generators operating at the same frequency (typically 1 kHz) and with a sinusoidal signal. In order to measure the current used by each DBD actuator, a resistor R was inserted between the lower electrodes and the ground. The potentials applied to the electrodes and the currents of the discharges were visualized on an oscilloscope and recorded.

In order to avoid spark discharges between the two upper electrodes, both high voltages applied to these electrodes must be synchronized. For that, the function generators were synchronized by a synchronizer working at the same frequency.

Each DBD actuator produced an electric wind in opposite direction. The conjunction of both electric winds produced two eddies rotating in opposite direction and built up a jet whose orientation depended on the voltage amplitude applied to each DBD actuator (figure 78).

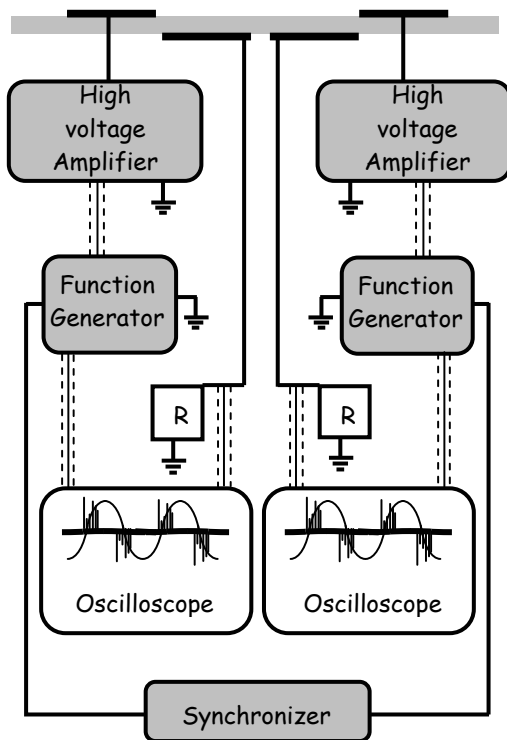


Fig. 77. Electrical circuit.

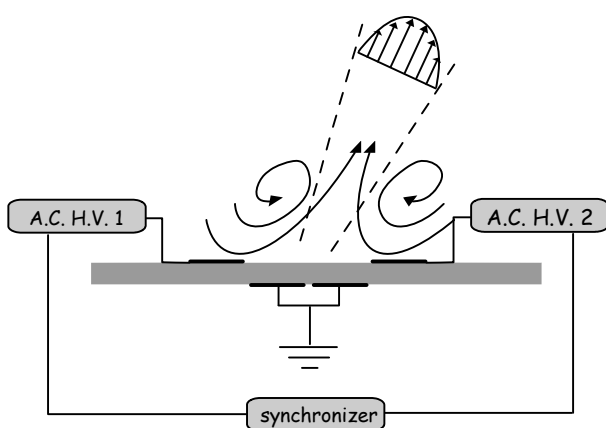


Fig. 78 Side view of the actuators

E. Actuators performing arc discharges

1) Spark synthetic jet actuator

This device has been performed and tested by several authors, but is well described by Caruana [55]. It is made of a 2 mm thick copper electrode having an aperture

whose diameter is in the range 0.3 mm to 1.5 mm. A second electrode, made of tungsten, is 1 mm in diameter. The copper electrode is grounded while the tungsten electrode is connected to a high voltage source. A spark occurred inside a cavity surrounded by alumina (figure 79). A distance of 2 mm exists between the electrodes. The alumina cavity diameter was 4 mm.

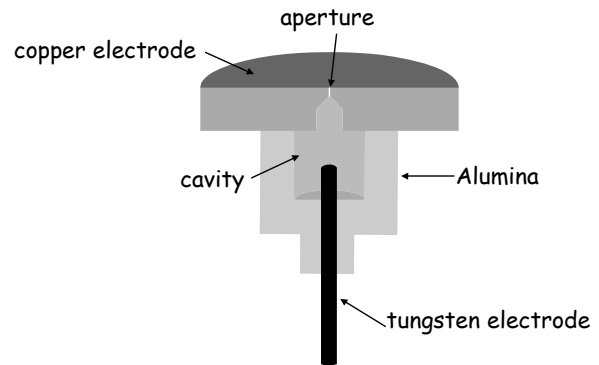


Fig. 79. Spark synthetic jet actuator.

The spark between the electrodes rises very fast the air temperature in the cavity. Then the pressure increasing the air is ejected through the aperture. When the temperature decreases, air is sucked in the cavity and the spark could occur again. Very high velocities (several hundreds m/s) could be reached for a 1mm in diameter aperture. The jet duration is between 200 and 300µs. Frequency repetition could reach 1 kHz during one set of experiments.

2) Arc filament actuators

An actuator has been performed by Samimy and al [56, 57] in order to modify high velocity jet. The goal was to control high-speed flows. Experiments were made on a jet plume exiting a 25.4 mm in diameter nozzle (figure 80). The compressed air was supplied to a stagnation chamber and conditioned before entering an axisymmetric converging-diverging nozzle. The air was then discharged horizontally through the nozzle into an anechoic chamber. The jet Mach number was up to 1.3.

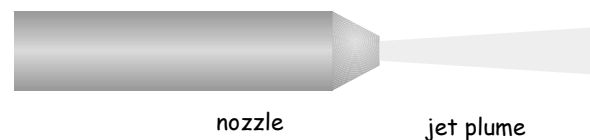


Fig. 80. Nozzle and jet.

Height uniformly distributed actuators are inserted in a ceramic (boron nitride) nozzle extension (figure 81). Each actuator is made of two tungsten 1 mm in diameter electrodes. The electrodes are inserted into the extension through radial channels. The electrodes tips in contact with the jet are housed in a ring groove made in the ceramic in order to reduce the effect of the jet on the discharge. The ring groove is 0.5 mm deep and 1mm wide. The distance between the two electrodes of each actuator is 3 mm. The basic working process of such actuator is to produce fast and intense arcs in order to

affect the flow by localized perturbations produced by arc-generated pressure/temperature spikes.

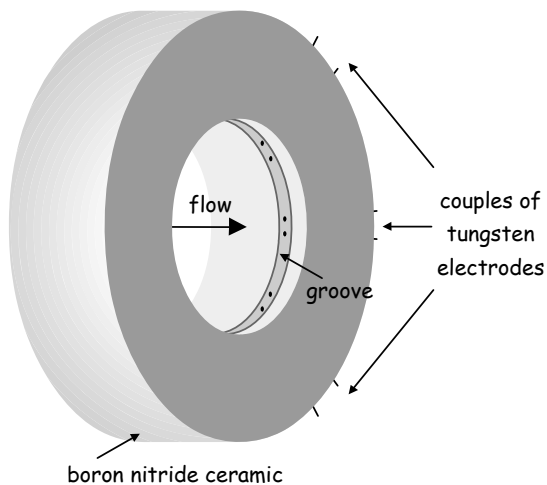


Fig. 81. Nozzle extension with the arc actuators.

Two DC 10 kV, 1 A, power supplies (Glassman High Voltage) were used to energized the eight actuators. Each of them was connected to a ceramic capacitor and a 15 k Ω high power solid body ceramic ballast resistor. The other extremity of the resistor is connected to a fast response, high repetition rate, high voltage MOSFET transistor switch (Behlke Power Electronics GmbH). The other extremity of the switch is also connected to the same kind of resistor itself connected to one electrode of one actuator. The other electrodes of each actuator are grounded. The eight switches are controlled with an 8-channels digital-to-analog output PCI card connected to a computer (figure 82). The switches could commute high voltage (up to 10 kV) at a variable repetition rate (up to 200 kHz) with a short rise/fall time ($\sim 0.1 \mu\text{s}$). The repetition rate and the duty cycle could be adjusted differently for each actuator with the computer through the PCI card.

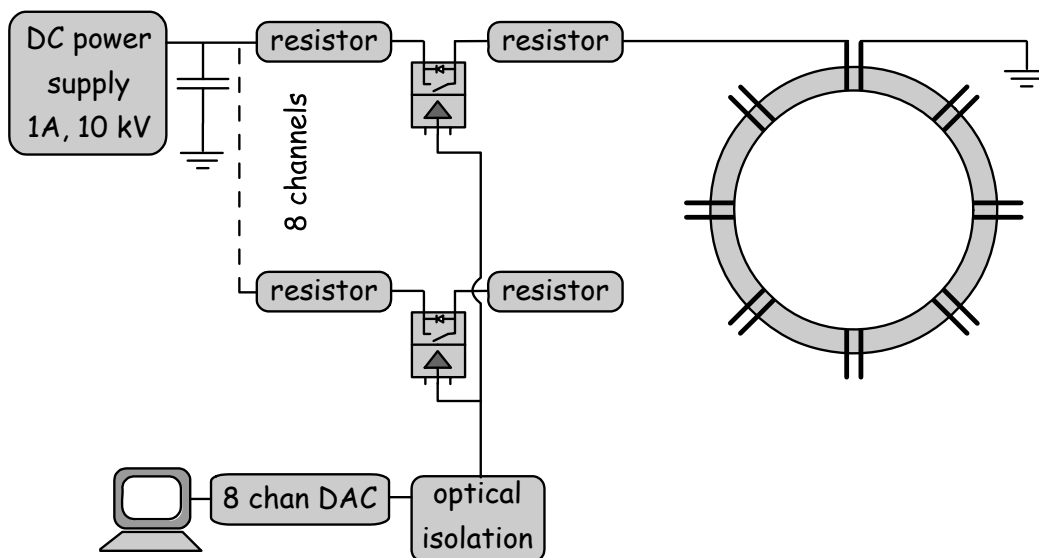


Fig. 82. Electrical setup for arc filament actuator.

Such set of arc actuator seems to be able to make important flow modifications. Its efficiency was analyzed in terms of repetition rate. The response was optimum at around 5 kHz this was consistent with the preferred-mode Strouhal number for such experiments which mostly seemed to correspond to a frequency of 4.5 kHz.

3) Surface sliding arc actuator

This actuator was first performed by Mizuno [58] (figure 83 and figure 84). It is composed of a mica sheet 0.4 mm thick under which a magnet (neodym, iron, boron) was stuck. The magnet (1.1 Tesla) is 22 mm in diameter and 10 mm thick. On the upper side of the mica sheet two triangular electrodes were stuck. One electrode is connected to AC High Voltage supply. The other one is grounded. For low voltage amplitude an arc discharge appeared between the closest parts of the electrodes. Due to the current in the arc discharge and to the magnetic field a force shifted the arc into one direction depending

on the polarity of the HV source. Another setup has been tested with tungsten wires and a periodic ramp High Voltage applied [59] (figure 85). The goal with these setups is to perform a kind of slippery wall in an alternating or constant direction.

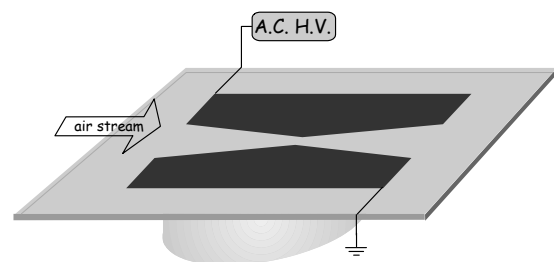


Fig. 83. General view of the actuator with triangular electrodes.

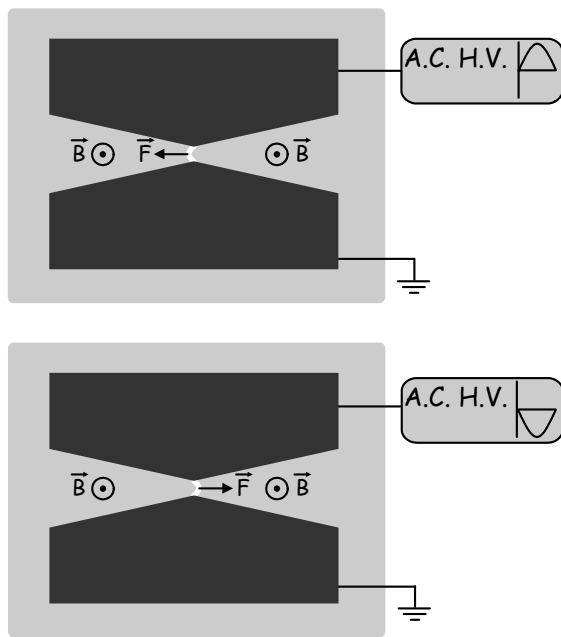


Figure 84. Upper view of the actuator with triangular electrodes.

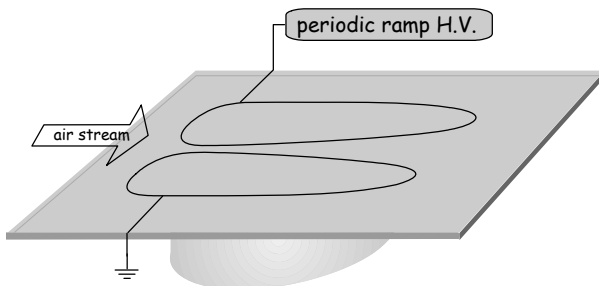


Fig. 85. General view of the actuator with tungsten wire electrodes.

V. DISCUSSION

Most of the plasma actuators (apart the arc filament and the surface sliding arc) used the electric wind generated by the discharge. Looking at the specific velocity perform by all these actuators we notice that the maximum velocity realized, up to now, is in the order of 10 m/s and even often smaller. Thus, obviously, in the present state of plasma actuators development, actuation due to only a permanent blowing or suction with such actuators will never be able to reattach flow on a body flying at a transonic velocity. Then, the perspectives of these actuators are to generate instabilities which could enhance vortices already existing in the boundary layer and whose development could totally change the boundary layer structure.

Indeed, the great advantage of this kind of actuators is their very fast response (Forte et al [60]). Thus, they can be used, as we have seen above, at a working frequency corresponding to the typical Strouhal number of the flow around the body experimented. In a near future it can be used at a right place, coupled with a sensor and acting at the right time in a special way to help the development of

specific flow structures which will radically change the boundary layer in the required configuration.

VI. CONCLUSION

In this paper, the aerodynamic phenomena still faced by aeronautic industry have been first presented and the different control techniques or devices already used or tested in the past have been described. Then, a special focus has been put on plasma actuators. These actuators know recently (for about ten years) a very intense interest due to their fast response and their simple and robust conception. The development of such actuators has been possible with new technologies in plasma generation and flow analysis now available as well as a better understanding of electrical discharges behavior. From this overview of plasma actuators conceptions and working ways, it seems that the perspectives of such actuators in the field of aerodynamic control for aeronautics are to act on aerodynamic structures already existing in the boundary layer and to favor their enhancement in order to provoke the flow modifications required.

REFERENCES

- [1] K. Takashima, N. Zouzou, E. Moreau, A. Mizuno and G. Touchard, "Generation of extended surface barrier discharge on dielectric surface – electrical properties", *IJPEST*, Vol. 1, No 1, pp. 14-20, 2007
- [2] H. Schlichting, "Boundary layer theory", Mc Graw Hill, 1955
- [3] R. Comolet, "Mécanique expérimentale des fluides", Masson, 1994
- [4] A. Betz, "Verfahren zur direkten Ermittlung des profilwiderstandes", *ZFM*. 16, pp. 42, 1925
- [5] B.M. Jones, ""The measurement of profile drag by the pitot traverse method", *ARC R&M* pp. 1688, 1936
- [6] N. Jacobs, K.E. Ward, & R. M. Pinkerton, "The characteristics of 78 related airfoil sections from tests in the variable-density wind tunnel", *NACA Report* No. 460, 1933
- [7] C. Wieselsberger, "Der Luftwiderstand von Kugeln" *ZFM*. 5, pp. 140-144, 1914
- [8] M. Gad-el-Hak, "Flow control, passive, active and reactive flow management", Cambridge University Press, 2000
- [9] M.J. Walsh and A. M. Lindemann, "Optimisation and Application of Riblets for Turbulent Drag Reduction", *AIAA paper*, No. 84-0347, 1984
- [10] D.M. Bushnell and J. N. Hefner, "Viscous Drag Reduction in Boundary Layers", *AIAA*, 1990
- [11] O. Schrenk, "Grenzschichtabsaugung", *Luftwissen* 7, 409, 1940
- [12] E. Moreau, "Airflow control by non thermal plasma actuators", *J. Phys. D: Appl. Phys.* 40, pp. 605-636, 2007
- [13] H. Velkoff and J. Ketcham, "Effect of an Electrostatic Field on Boundary-Layer Transition", *AIAA J.*, 16, pp. 1381-1383, 1968
- [14] M.R. Malik, L. Weinstein and M. Hussaini, "Ion Wind Drag Reduction", *AIAA paper* # 1983-0231, 1983
- [15] F. Soetomo, "The influence of high voltage discharge on flat plate drag at low Reynolds number flow", M.S. thesis, Iowa States University, 1992
- [16] F. Soetomo and G.M. Colver, "Effect of a corona discharge on boundary layer growth", *Electrostatics Society of America Conference*, 1993

- [17] F. Soetomo, G.M. Colver and K. Forouraghi, "Micro-Force Measurements of drag on a Small Flat Plate in the Presence of a Corona Discharge", Société Française d'Electrostatique Conference, pp. 55-60, 2004
- [18] S. El-Khabiry and G.M. Colver, "Drag reduction by DC corona discharge along an electrically conductive flat plate for small Reynolds number flow", *Phys. Fluids*, 9 pp. 587-599, 1997
- [19] G.M. Colver and S. El-Khabiry, "Modelling of DC Corona Discharge Along an Electrically Conductive Plate with Gas Flow", *IEEE Trans. Indust. Apl.* 35, pp. 387-394, 1999
- [20] C. Noger, "Etude expérimentale de la modification de l'écoulement autour d'un cylindre circulaire en injectant des charges électriques par le principe de la décharge corona (Application à l'aéronautique)", M.S. thesis, Université de Poitiers, 1996
- [21] C. Noger, G. Touchard and J.S. Chang, "Active controls of electrohydrodynamically induced secondary flow in corona discharge reactor", ISNTPT-2, pp. 136-141, 1997
- [22] G. Touchard, "Les plasmas froids dans le contrôle des écoulements subsoniques", 39^{ème} Colloque d'aérodynamique appliquée, Contrôle des écoulements, 2004
- [23] G. Artana, G. Desimone, G. Touchard, "Study of the changes in the flow around a cylinder caused by electroconvection", Inst. Phys. Conf. Ser. No 163, pp. 147-152, 1999
- [24] G. Desimone, G. Diprimio, G. Artana, "Modifications to the flow field around a cylinder by means of electrodes placed on its surface", Société Française d'electrostatique Conference, pp. 80-84, 1999
- [25] L. Léger, E. Moreau, G. Artana and G. Touchard, "Influence of a DC corona discharge on the airflow along an inclined flat plate", *J. of Electrostatics*, 50-51, pp. 300-306, 2001
- [26] G. Artana, G. Diprimio, G. Desimone, E. Moreau, G. Touchard, "Electrohydrodynamic actuators on a subsonic airflow around a circular cylinder", Proc. 4th AIAA Weakly Ionized Gases International Conference, paper # 2001-3056, 2001
- [27] G. Artana, J. D'Adamo, L. Léger, E. Moreau, G. Touchard, "Flow Control with Electrohydrodynamic Actuators", Proc. 39th AIAA Meeting, paper #2001-0351, 2001
- [28] J. D'Adamo, G. Artana, E. Moreau, G. Touchard, "Control of the airflow close to a plate with electrohydrodynamic actuators", Proc. ASME, paper # 2002-31041, 2002
- [29] G. Artana, J. D'Adamo, L. Léger, E. Moreau, G. Touchard, "Flow Control with Electrohydrodynamic Actuators", *AIAA Journal*, 40, 9, pp. 1773-1779, 2002
- [30] K.T. Hyun, "The wake flow control behind a circular cylinder using ion wind", *Experiments in Fluids*, 35, pp. 541-552, 2003
- [31] E. Moreau, L. Léger, G. Touchard, "Effect of a DC surface non-thermal plasma on a flat plate boundary layer for airflow velocity up to 25 m/s", *J. of Electrostatics*, 64, pp. 215-225, 2006
- [32] L. Léger, E. Moreau, G. Touchard, "Electrohydrodynamic airflow control along a flat plate by a DC surface corona discharge – Velocity profile and wall pressure measurements", Proc. 1st AIAA Flow Control Conference, paper # 2002-2833, 2002
- [33] L. Léger, E. Moreau, G. Touchard, "Effect of a DC corona electrical discharge on the airflow along a flat plate", *IEEE Trans. Indust. Appl.*, 38, 6, pp. 1478-1485, 2002
- [34] L. Léger, E. Moreau, G. Touchard, "Control of low velocity airflow along a flat plate with a DC electrical discharge", IEEE-IAS Conference, Chicago, (CD-Rom), 2001
- [35] R. Sosa, E. Moreau, G. Touchard, G. Artana, "Stall control at high angle of attack with periodically excited EHD actuators", AIAA Meeting, paper # 2004-2738, 2004
- [36] R. Sosa, G. Artana, "Steady control of laminar separation over airfoils with plasma sheet actuators", *J. of Electrostatics*, 64, pp. 604-610, 2006
- [37] R. Sosa, E. Moreau, G. Touchard, G. Artana, "Stall control at high angle of attack with plasma sheet actuators", *Experiments in fluids*, 42, pp. 143-167, 2006
- [38] E. Moreau, L. Léger, G. Touchard, "Three phase travelling wave surface discharge along an insulating flat plate in air: application to electrohydrodynamically airflow control", IEEE-CEIDP Conference, pp. 822-826, 2002
- [39] J. Pons, E. Moreau, G. Touchard, "Electrical and aerodynamic characteristics of atmospheric pressure barrier discharge in ambient air", ISNTPT-4, pp. 307-310, 2004
- [40] J. Pons, E. Moreau, G. Touchard, "Asymmetric surface barrier discharge in air at atmospheric pressure: electric properties and induced airflow characteristics", *J. Phys. D : Applied Physics* 38, pp. 3635-3642, 2005
- [41] J. Pons, E. Moreau, G. Touchard, "Surface DC corona discharge and AC barrier discharge in air at atmospheric pressure: measurement of the induced ionic wind velocity", 15th Conference on Gas discharge and their Applications, 2004
- [42] M. Forte, J. Jolibois, E. Moreau, G. Touchard, M. Cazalens, "Optimization of a dielectric barrier discharge actuator by stationary and instationary measurements of the induced flow velocity, application to airflow control", AIAA Meeting paper # 2006-2863, 2006
- [43] E. Moreau, C. Louste, G. Touchard, "Electric wind induced by sliding discharge in air at atmospheric pressure", *J. of Electrostatics*, 66, pp. 107-114, 2008
- [44] J.R. Roth, D.M. Sherman and S.P. Wilkinson, "Boundary layer flow control with a one atmosphere uniform glow discharge surface plasma", AIAA Meeting conference paper # 98-0328, 1998
- [45] J.R. Roth, "Aerodynamic flow acceleration using paraelectric and peristaltic electrohydrodynamic effect of a One Atmosphere Uniform Glow Discharge", *Phys. Plasmas*, 10, 5, pp. 2117-2126, 2003
- [46] J.R. Roth, H. Sin, C. M. Madhan and S. P. Wilkinson, "Subsonic plasma aerodynamics using Lorentzian momentum transfer in atmospheric normal glow discharge plasmas", 55th APS Gaseous Electronic Conference, paper YF2-004, 2002
- [47] T.C. Corke, C. He and M.P. Patel, "Plasma flaps and slats: Application of weakly-ionized plasma actuators", AIAA Meeting, paper # 2004-2127, 2004
- [48] D.F. Opaits, D.V. Roupasov, A.Y. Starikovskaia, A. Yu. Starikovskii, I.N. Zavalov, S.G. Saddoughi, "Plasma control of boundary layer using low temperature non equilibrium plasma of gas discharge", AIAA Meeting, paper # 2005-1180, 2005
- [49] F.O. Thomas, A. Kozlov and T. Corke, "Plasma actuators for bluff body flow control", AIAA Meeting, paper # 2006-2845, 2006
- [50] K.S. Choi, J.R. DeBisschop and B.R. Clayton, "Turbulent Boundary-Layer Control by Means of Spanwise-Wall Oscillation", *AIAA Journal*, 36, 7, pp. 1157-1163, 1998
- [51] S.P. Wilkinson, "Investigation of an oscillating surface plasma for turbulent drag reduction", AIAA Meeting, paper #2003-1023, 2003
- [52] T.N. Jukes., K-S Choi, G.A. Johnson and S. Scott, "Turbulent Drag Reduction by Surface Plasma through Spanwise Flow Oscillation", AIAA Meeting, paper # 2006-3693, 2006
- [53] A. Santhanakrishnan, and J.D. Jacob, "On Plasma Synthetic Jet Actuators", AIAA Meeting, paper #2006-0317, 2006
- [54] N. Bénard, J. Jolibois, E. Moreau, R. Sosa, G. Artana, G. Touchard, "Aerodynamic plasma actuators: A directional micro-jet device", *Thin Solid Films*, in press (available on line), 2007
- [55] D. Caruana, "Générateur de micro-jet synthétique par plasma", GDR contrôle de décollement, No 2, 2006
- [56] M. Samimy, J.H. Kim, J. Kastner, I. Adamovich and Y. Utkin, "Active control of high-speed and high-Reynolds-number jets using plasma actuators", *J. Fluid Mech.*, vol; 578, pp. 305-330, 2007
- [57] Y.G. Utkin, S. Keshav, J.H. Kim, J. Kastner, I.V. Adamovich and M. Samimy, "Development and use of localized arc filament plasma actuators for high-speed flow control", *J. Phys. D: Appl. Phys.*, 40, pp. 685-694, 2007
- [58] A. Mizuno, "Development of a plasma flow control actuator using a magnetic field", *LEA internal report*, 2007
- [59] G. Touchard, N. Benard, "Mise au point d'un nouveau type d'actionneur aérodynamique à plasma utilisant un champ

magnétique", *LEA internal report*, 2007

- [60] M. Forte, L. Léger, J. Pons, E. Moreau, G. Touchard, "Plasma actuators for airflow control: measurements of the non-stationary induced flow velocity", *J. of Electrostatics*, 63, 6-10, pp. 929-936, 2005